도시계획학 석사학위논문

Analysis of Spatial and Temporal Gross Primary Productivity and Evapotranspiration in Korea by Using BESS

BESS를 이용한 한반도 광합성과 증발산의 시공간 패턴 분석

2013년 2월

서울대학교 환경대학원

환경계획학과

전 수 현

Analysis of Spatial and Temporal Gross Primary Productivity and Evapotranspiration in Korea by Using BESS

BESS를 이용한 한반도 광합성과 증발산의 시공간 패턴 분석

지도교수 이 도 원

이 논문을 도시계획학 석사학위 논문으로 제출함

2012년 10월

서울대학교 환경대학원

환경계획학과

전 수 현

전수현의 도시계획학 석사 학위논문을 인준함

2012년 12월

위 원 장 (인)

부위원장 (인)

위 원 (인)

Abstract

Analysis on spatial and temporal patterns of gross primary productivity (GPP) and evapotranspiration (ET) is critical in understanding and predicting terrestrial carbon and water cycles. However, there have been a few studies which provide spatially and temporally continuous estimates of GPP and ET in the Korean Peninsula. In this study, spatial and temporal patterns of GPP and ET in the Korean Peninsula were studied by using a bio-physical model, Breathing Earth System Simulator (BESS).

GPP and ET from BESS are sensitive to Leaf Area Index (LAI) which is one of important input variables of BESS. LAI refinement was conducted by using re-modified temporal and spatial filter (rTSF) and LAI refinement improved accuracy compared to LAI from BESS and raw MODIS. The simulations of 11-year (2001-2011) GPP and ET in the Korean Peninsula were performed by using refined LAI. BESS derived GPP and ET were verified with eddy covariance measurements at 4 sites and 5 sites, respectively. Also, BESS derived basin ET was evaluated against water balance derived ET at a basin scale. Both GPP and ET from BESS show high positive bias at GDK and GCK sites while BESS derived GPP and ET were comparable to eddy covariance measurement at other sites and water balance derived ET.

The mean annual land GPP and ET over the eleven years (2001-

2011) were 1,183 gC m^{-2} $year^{-1}$and 491 mm $year^{-1}$. Land cover change was one of major causes for interannual variation of GPP and ET. In dry year, ET at highland became more sensitive to canopy conductance than that in normal year. Spring and autumn droughts caused spring and autumn ET to become most sensitive to canopy conductance. The sensitivity of ET to available energy increased in summer due to clouds during the summer monsoon.

Key words: Gross Primary Productivity (GPP), Evapotranspiration (ET), Breathing Earth System Simulator (BESS), Flux measurement.

학번 : 2011-22331

<Contents>

I. Introduction

Monitoring land-atmosphere interactions has a growing importance in research communities. Biosphere-atmosphere interactions such as Gross Primary Productivity (GPP) and Evapotranspiration (ET) can be monitored through field measurements or remote sensing techniques. Equipment used for field measurements include: eddy-covariance system [*Baldocchi et al.*, 2001] and portable gas exchange system such as LI-6400 (http://www.licor.com). Interactions between land and atmosphere such as GPP and ET can be estimated in satellite images taken by Moderate Resolution Imaging Spectroradiometer (MODIS) (http://modis.gsfc.nasa.gov) [*Mu et al.*, 2007; *Ryu et al.*, 2011; *Zhao et al.*, 2005].

Field measurements and satellite data have their respective advantages and limitations. Field measurements serve as "ground-truths" data [*Hoover*, 2008]. For example, eddy covariance data (flux tower data) enable us to evaluate MODIS products of GPP and evaporation [*Baldocchi et al.*, 2001]. However, in-situ observations are limited in terms of spatial coverage [*Jung et al.*, 2010]. Typical footprints of eddy-covariance system cover hundred meters to several kilometers [*Schmid*, 1994]. The global network of eddy covariance system (http://fluxnet.ornl.gov) spreads over 500 sites around the world but is mostly located in North America and Europe.

Regional to global scale of remotely sensed data enhance monitoring of terrestrial ecosystems. Remote sensing measurements provide spatially continuous data which cannot be achieved with field measurements. However, the accuracy of the remotely sensed land surface properties depends on atmospheric conditions such as clouds and aerosol [*Kobayashi and Dye*, 2005]. For example, MODIS derived LAI values tend to be low under cloudy conditions [*Myneni et al.*, 2002; *Zhao et al.*, 2005]. In East Asia, MODIS LAI estimates might be underestimated during the summer monsoon period when clouds appear frequently. Also, erroneous output can be derived from incorrect algorithms in MODIS product. In case of MODIS GPP (MOD17), it underestimates at high productivity and overestimates at low productivity due to simple algorithms of Light Use Efficiency (LUE) [*Heinsch et al.*, 2006; *Zhang et al.*, 2012]. LUE in computation of MODIS GPP is derived from a look-up table but original estimation of LUE may contain errors. LUE is improperly characterized due to coarse resolution of environmental stress factors which may lead to errors in its estimation [*Sims et al.*, 2008; *Wu et al.*, 2010]. Big leaf model is used in MODIS GPP algorithm and it was found that a big leaf model underestimates GPP due to unrepresented shade leaves [*de Pury and Farquhar*, 1997]. Also, spatial resolutions between meteorological and terrestrial input data are very different and this could lead to bias in MODIS GPP [*Heinsch et al.*, 2006; *Ryu et al.*, 2011; *Yuan et al.*, 2010; *Zhao et al.*, 2005].

Integration of field measurement and satellite based measurement is critical in monitoring carbon and water fluxes over large areas [*Running et al.*, 1999]. Many models have been developed, by taking advantages from both measurements. Field measurements provide point data. Models can be evaluated and improved on the points where field measurements exist [*Baldocchi et al.*, 1996]. Remote sensing offers spatially continuous model input data [*Fang et al.*, 2007; *Schwarz and Zimmermann*, 2005] thus model can produce spatially continuous outputs. Integrating these input datasets into a model makes it possible to monitor the unmeasured ecosystem [*Running et al.*, 1999].

Farquhar's leaf-level photosynthesis model [*Farquhar et al.*, 1980] has been widely used in many terrestrial carbon cycle models [*Cramer et al.*, 2001; *Sitch et al.*, 2008]. However, remote sensing derived GPP models mostly rely on the empirical light use efficiency approach [*Cramer et al.*, 1999; *Turner et al.*, 2003]. ET has been estimated from the water balance [*Rodell et al.*, 2004], the Penman-Monteith equation [*Cleugh et al.*, 2007; *Mu et al.*, 2007; *Ryu et al.*, 2011] or energy balance residual [*Allen et al.*, 2007; *Norman et al.*, 1995; *Su*, 1999; *Yeh et al.*, 1998]. However, few studies using remote sensing data attempt to couple carbon and water fluxes [*Ryu et al.*, 2011] although carbon and water cycle are inherently coupled via stomata [*Baldocchi*, 1997; *Leuning et al.*, 1995].

The Breathing Earth System Simulator (BESS) used in this study couples carbon and water fluxes and uses dual-source (canopy and soil) and two-leaf model (sunlit and shaded leaves). It is a biophysical model that combined Farquhar's photosynthesis model and Penman-Monteith evaporation model using MODIS, and quantifies GPP and ET with a spatial resolution of 1 – 5 km and a temporal resolution of 8 days [*Ryu et al.*, 2011]. Both GPP and ET estimates from BESS are sensitive to LAI value [*Ryu et al.*, 2011] which imply that high quality of LAI data is essential in accurate estimates of GPP and ET.

MODIS LAI data are reprocessed in BESS. BESS uses MODIS LAI data classified as "Main (RT) method used, best result possible (no saturation)" or "Main (RT) method used with saturation. Good, very usable" in the quality flags (filtered data). The filtered data of 5 years (2001-2005) are averaged pixel by pixel (5-year-averaged data). When the values of filtered data are lower than half of 5-year-averaged data values, filtered data are removed and replaced by the 5-year-averaged data. However, this approach can reduce inter-annual variation of LAI, and can substantial noise in LAI estimates during the summer. Also, 5-year-averaged data could be still very low during the summer monsoon season. Therefore, improvement of MODIS LAI product is required in order to better quantify GPP and ET.

Analysis on spatial and temporal patterns of GPP and ET is

important in understanding and predicting terrestrial carbon and water cycles. Analyzing GPP and ET in spatial and temporal domain enables us to understand environmental factors that control GPP and ET in different time and region [Bubier et al., 2003; Turner et al., 2004]. Through this, better prediction of spatial and temporal responses of carbon and water cycle under a changing climate can be achieved. Also, better understanding of spatial and temporal patterns of GPP and ET could enhance carbon and water managements to prepare carbon market era and secure sustainable water resources [*Running et al.*, 1999]. Therefore, analyzing spatial and temporal variations of carbon and water fluxes is needed.

There have been a few studies which provide spatially and temporally continuous estimates of GPP and ET in the Korean Peninsula. Monitoring of carbon and water cycle in Korea has been done mostly in plot, catchment or river basin scale. *Lee et al.* [2010] studied ET derived from precipitation and discharge data and GPP estimated via water use efficiency in Han River basin. In a deciduous broadleaf forest watershed in the Gwangneung Experimental Forest, carbon fluxes (wood biomass productions) during 1991-2004 were quantified [*Kim et al.*, 2010]. Some studies used eddy-covariance data in analyzing carbon [*Hong and Kim*, 2011; *Kwon et al.*, 2010; *Kwon et al.*, 2009] and water fluxes [*Hong et al.*, 2008; *Kang et al.*, 2012]. *Hwang et al.* [2008] used Regional Hydro-Ecological Simulation System to evaluate drought effect on MODIS GPP in GEF.

There are a few studies on nationwide carbon and water fluxes. *Choi et al.* [2002] quantified carbon uptake of Korean forests by using forest tree inventory data collected from 3500 permanent plots. Trend of ET during 1968-2001 in Korea was estimated via The Precipitation-Runoff Modeling System [*Bae et al.*, 2008]. However, spatial analysis is hard to be done with point data [*Choi et al.*, 2002] or area data [*Bae et al.*, 2008]. Compared to point data and area data, pixel based data is better in detailed (less than regional scale)-spatial analysis.

BESS was evaluated in 33 eddy flux tower sites located from arctic to tropical regions [Ryu et al., 2011]. However, the performance of BESS in the Korean Peninsula has never been evaluated. In order to achieve reliable quantification of GPP and ET in the Korean Peninsula, BESS should be evaluated with various data stream such as data from eddy-covariance system and basin water balance data.

This study has three main objectives. Firstly, BESS is going to be evaluated with various data stream and be improved. In this part, the following tasks will be done: 1) To evaluate BESS derived GPP and ET estimates, and 2) To improve MODIS LAI product, one of the important variables in BESS. Secondly, spatial and temporal patterns of GPP and ET in the Korean Peninsula are going to be analyzed. In this part, the following tasks will be done: 1) To quantify GPP and ET of the Korean Peninsula

during 2001-2011, using BESS, and 2) To analyze spatial and temporal patterns of GPP and ET. Lastly, I am going to answer the following questions: 1) what controls ET in the Korean Peninsula, and 2) How contributions of sunlit and shaded leaves to GPP vary with the seasons.

II. Methods

1. Site description

The Korea Peninsula is located in temperate region (warm temperate, winter dry and hot summer [Kottek et al., 2006]). The average annual temperature of Korea during the last three decades is 10 ~ 15 ℃. The average of annual rainfall during the last three decades is about 1350 mm, more than half of which occurs in summer. The relative humidity in spring (Mar, Apr and May) is around 64% while that in summer (Jun, Jul and Aug) is about 78%. Korea has monsoon season which usually occurs from late June to late July (Korea Meteorological Administration, n.d.).

Five sites (GDK, GCK, HFK, Seolmacheon site (SMK), Cheongmicheon Farmland Site (CFK)) were used in evaluation of BESS. GDK, GCK and SMK are forest sites and dominant vegetation types are: deciduous broadleaf trees at GDK, evergreen coniferous trees at GCK and mixed forest at SMK. HFK and CFK are either farmlands or rice paddies (www.koflux.org). Elevation of SMK is highest (293 m a.s.l.), followed by GDK (260 m a.s.l.), CFK (141 m a.s.l.), GCK (128 m a.s.l.) and HFK (13.74 m a.s.l.). GCK, CFK and HFK have relatively flat terrain while GDK and SMK are on a slope (www.koflux.org).

Table 1 description of field measurement sites (source: www.koflux.org)

	GDK	GCK	HFK	SMK	CFK
Site name	KoFlux Gwangneung Supersite - Deciduous forest	KoFlux Gwangneung Supersite – Evergreen forest	KoFlux Haenam site	KoFlux Seolmacheon site	Cheongmicheon Farmland Site
Location	37° 45' N, 127° 9' E	37° 44'54.7" N, 127°09'46.6 " E	34.55° N, 126.57° E	37° 56' 19.99" N, 126° 57' 16.94" E	37° 9' 35" N, 127° 39' 10"E
Elevation	260m a.s.l	128 m a.s.l	13.74m a.s.l.	293 m a.s.l	141 m a.s.l.
Slope	Dominant slopes 10~20° max. 51°	Dominant slopes 0~20°	2°	N/A	0°
Terrain Type	Mountainous area	Mountainous area (relatively flat)	Relatively flat except the southeast section with a slope of about 4°	Complex terrain	Flat
Climate	Temperate : snow - winter dry - hot summer (Dwa)	Temperate : snow - winter dry - hot summer (Dwa)	humid subtropical (Cfa)	Temperate : snow - winter dry - hot summer (Dwa)	Warm Continental Climate (Dwa)
Vegetation type	Deciduous forest	Coniferous forest	Rice/Farm land	Mixed Forest	Rice paddy
Data	GPP ET LAI	GPP ET LAI	GPP ET	ET	ET
Data availability	2007, 2008, 2009, 2010,	2007, 2008, 2009, 2010	2006, 2008	2008, 2009, 2010	2008, 2009, 2010

2. Description of BESS

BESS consists of five key modules: atmospheric radiative transfer, canopy radiative transfer, canopy photosynthesis, canopy evapotranspiration and soil evaporation. In atmospheric radiative transfer module, an atmospheric radiative transfer model (FLiES) is used to calculate incoming shortwave radiation, photosynthetic active radiation (PAR) and near infrared radiation (NIR) at top of canopy [Iwabuchi, 2006; Kobayashi and Iwabuchi, 2008; Ryu et al., 2011]. Absorbed PAR, NIR and longwave radiation are quantified in canopy radiative transfer module, using LAI and clumping index. Maximum carboxylation velocity (Vcmax) is derived from albedo and nitrogen relation or the look-up table which classifies Vcmax values based on plant functional type (PFT) and climatic zones [Ryu et al., 2011]. Vcmax

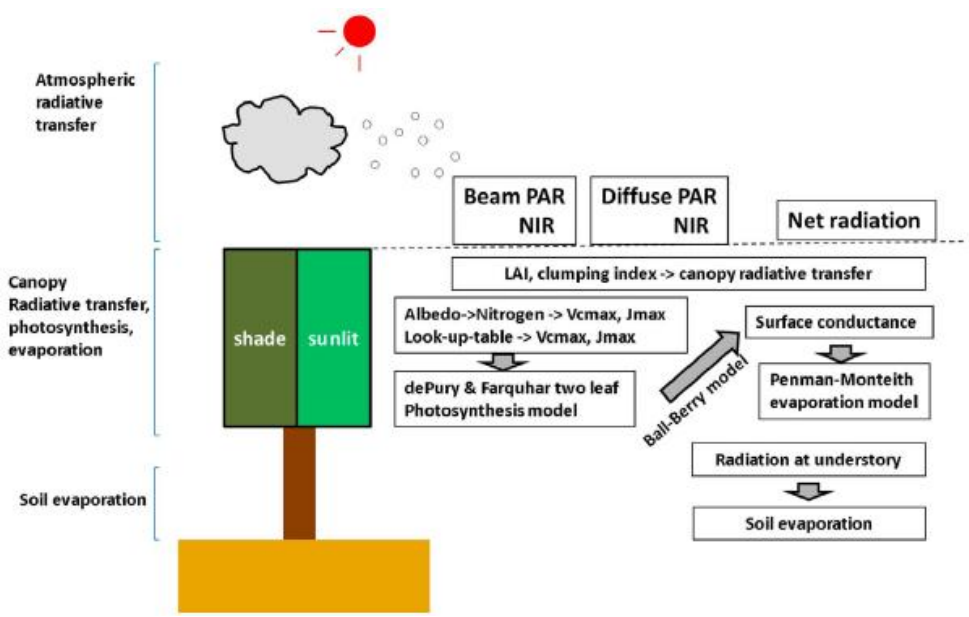

Figure 1 Overview of BESS [Ryu et al., 2011]

is a key parameter in the Farquha's photosynthesis model [Farquhar et al., 1980], used in quantification of photosynthesis in BESS. Based on the two-leaf canopy conductance and Penman-Monteith equation, evapotranspiration at canopy was quantified.

3. Improvement of BESS

1) Reprocessing MODIS LAI data

Fang et al. [2008] developed a temporal spatial filter (TSF) which aims to improve the quality of spatial and temporal series of MODIS LAI products over North America. Recently, mTSF (modified TSF) has been developed in order to improve MODIS LAI products globally [*Yuan et al.*, 2011]. mTSF differs from TSF in two parts. TSF processes data with QC $\geq$ 32 while QC of data processed in mTSF are greater than zero. With TSF, the mean values from the multi-year data are taken as background values. Gaps within the multi-year data are filled by using an improved ecosystem curve fitting (ECF) method based on the MODIS vegetation continuous fields product (VCF) (VCF-ECF). However, as VCF-ECF is difficult to apply towards LAI improvements on a global scale, mTSF uses a new algorithm consisting of the following five steps: Conditional multi-year average, TIMESAT Savitzky–Golay filter [*Jönsson and Eklundh*, 2004], Local Per Class Mean, Per Class Mean and multi-year Per Class Mean.

The mTSF still needs improvements. In summer, data with QC of zero shows very low value (less than 2) compared to ones with QC of 32 even when the dates are not far apart. Using data only with QC=0 could lower the improved LAI value during summer seasons which could lead to an underestimation of GPP and ET in many models. Also, up-down-up patterns of LAI value, defined as the increase of LAI in spring, followed by a decrease in summer and again an increase in the fall season, were found in multiple evergreen broadleaf forests (EBF), deciduous broadleaf forests (DBF), mixed forests

Table 2 MODIS LAI quality control (QC) value [*Ranga Myneni*, n.d.]

QC	MODIS LAI Algorithms
QC=0	Main (RT) algorithm used, with no cloud, no saturation
0<QC<32	Main (RT) algorithm used, with cloud or cloud state not definedb, no saturation
QC=32	Main (RT) algorithm used, with no cloud, saturation occurred
32<QC<64	Main (RT) algorithm used, with cloud or cloud state not defined, saturation occurred
64≤QC<96	Main algorithm failed due to bad geometry, back-up algorithm used
96≤QC<128	Main algorithm failed due to problems other than geometry, backup algorithm used
QC≥128	Pixel not produced at all, value couldn't be retrieved

(MF) and specifically, Gwangneung deciduous forest. This may be due to the fact that mTSF uses data only with QC=0 which leads to low background values in summer seasons. When background value in summer is low, up-down-up patterns occur.

MODIS land cover product is a key input data in the MODIS LAI algorithm which includes 5 types of schemes: IGBP global vegetation classification scheme, University of Maryland (UMD) scheme, MODIS-derived LAI/fPAR scheme, MODIS-derived Net Primary Production (NPP) scheme and Plant Functional Type (PFT) scheme [*Friedl*, n.d.]. The type 5 (PFT) is used as Look-Up-Table in MODIS daily LAI product (MOD15A1) and MOD15A1 is composite of MODIS 8day LAI product (MOD15A2) which is used in this study. Using land cover type 5 (PFT) in reprocessing MODIS LAI product could reduce the uncertainty which might occur during spatial filling.

Remodified TSF (rTSF) developed in this study overcomes the limitations of the mTSF. The rTSF is an enhancement over the mTSF in two different ways. 1) The rTSF uses data of which QC is 0 or 32. 2) The rTSF removes outliers. The rTSF calculates the mean of the top three values and the change value of each data against the adjacent. It then eliminates those data with a change value greater than half of the top three mean.

Table 3 Comparison of land cover and LAI data use, and computation steps among rTSF, mTSF [*Yuan et al.*, 2011] and TSF [*Fang et al.*, 2008]

		rTSF	mTSF	TSF
Land cover		MODIS land cover type 5 (PFT)	MODIS land cover type 5 (PFT)	MODIS land cover type 5 (PFT)
Background value computation	**QC value of Reference data**	QC= 0 or QC = 32	QC=0	QC<32
		1. Conditional multi-year average of reference data 2. Removing outliers 3. Temporal gap filling with Savitzky–Golay filters 4. Local Per Class Mean 5. Per Class Mean 6. Multi-year Per Class Mean 7. SG filter	1. Conditional multi-year average of reference data 2. TIMESAT SG filter 3. Local Per Class Mean 4. Per Class Mean 5. Multi-year Per Class Mean. 6. TIMESAT SG filter	1. Multi-year mean of reference data 2. ECF-VCF
Observation value computation	**QC value of Reference data**	QC= 0 or QC = 32	QC<128	QC<128
		1. Treat reference data as observation value 2. Removing outliers 3. Temporal gap filling with Savitzky–Golay filters 4. Local Per Class Mean 5. Per Class Mean 6. Multi-year Per Class Mean 7. SG filter	1. Treat reference data as observation value 2. Temporal filter (SG filter) to fill gaps	1. Treat reference data as observation value 2. Temporal filter (SG filter) to fill gaps

① Basic concept of rTSF.

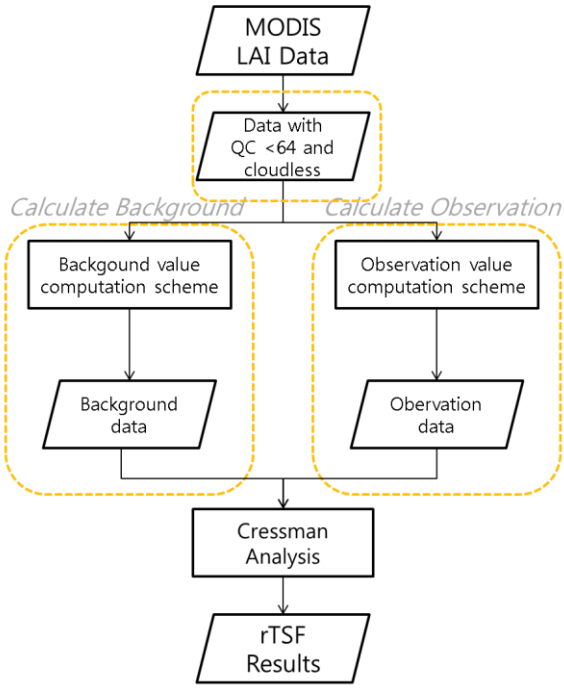

Figure 2 Flow chart of rTSF prcesses. Processes in dashed box are different from those of mTSF.

The rTSF uses data with QC = 0 or 32 as reference data for reprocessing. Figure 2 shows a flowchart of rTSF which uses a linear combination of background and observation value as the TSF and the mTSF do. Background value is “predicted value” based on multi-year MODIS LAI datasets while observation value is “observed value” showing MODIS LAI value of one year. Observed value is important in interannual variation of improved MODIS LAI data.

The rTSF process can be divided into four parts. 1) Eliminating data with QC ≠ 0 or 32. 2) Calculating the background value based on the background value computation scheme explained in section ④ background value computation. 3) Calculating the observation value based on observation value computation scheme explained in section ⑤ observation value computation. 4) Determining the final value by applying the calculated background value and observation value to Cressman analysis (section ②). Background value for each pixel on the same DOY has similar value over multiple years and affects the overall shape of the time series of LAI. Observation value influences interannual variation.

② Cressman analysis

Cressman analysis is an interpolation method through which background gridpoint value (predicted value) is corrected by a linear combination of residuals between background value and observation value (Eq. 1) [*Cressman,* 1959]. Weighting function depends on the distance between gridpoint and observation (Eq. 2).

$$X_a(r_i) = X_b(r_i) + \sum_{j=i-n}^{i+n} W(r_i, r_i)[X_o(r_i) - x_b(r_j)] / \sum_{j=i-n}^{i+n} W(r_i, r_i) \quad \text{(Eq. 1)}$$

$W(r_i, r_i)=\max(0,(R^2-d^2_{i,j})/ (R^2+d^2_{i,j}))$ (Eq. 2)

Eq.(1), where r_i and r_j are the location of data values, X_b and X_o are background and observation value, respectively. X_a is final value and $W(r_i, r_i)$ is weighting function which depends on distance ($d_{i,j}$) between points r_i and r_j. R is set as 24.

③ Data processing

The mTSF processes the MODIS LAI data with QC >0 from 2000 to 2011. However, it has been known that data with QC<32 tend to show low value in the summer season (figure 3). Therefore, using data only with QC<32 could lead to an underestimation of LAI. For these reasons, data processed in the rTSF are ones with QC≠0 and QC≠32.

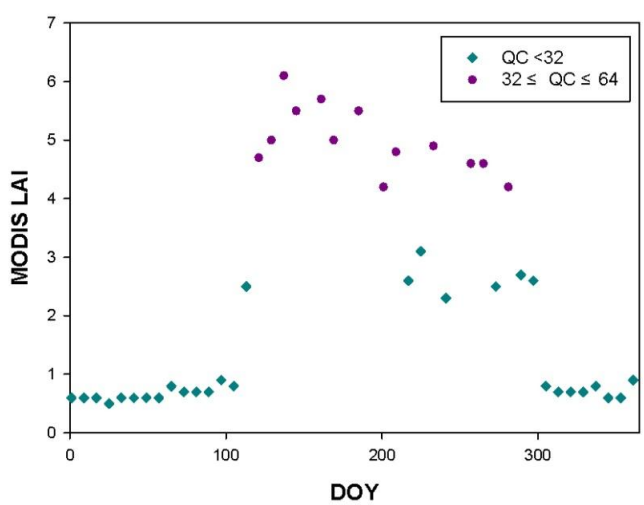

Figure 3 MODIS LAI with QC < 32 shows low values, compared to MODIS LAI with 32 ≤ QC ≤ 64 (year: 2005, Gwangneung deciduous forest).

④ Background value calculation

Background value calculation is based on that of the mTSF [*Yuan et al.*, 2011]. However, steps 1, 3 and 4 are modified and step 2 is added to minimize the frequency of up-down-up patterns.

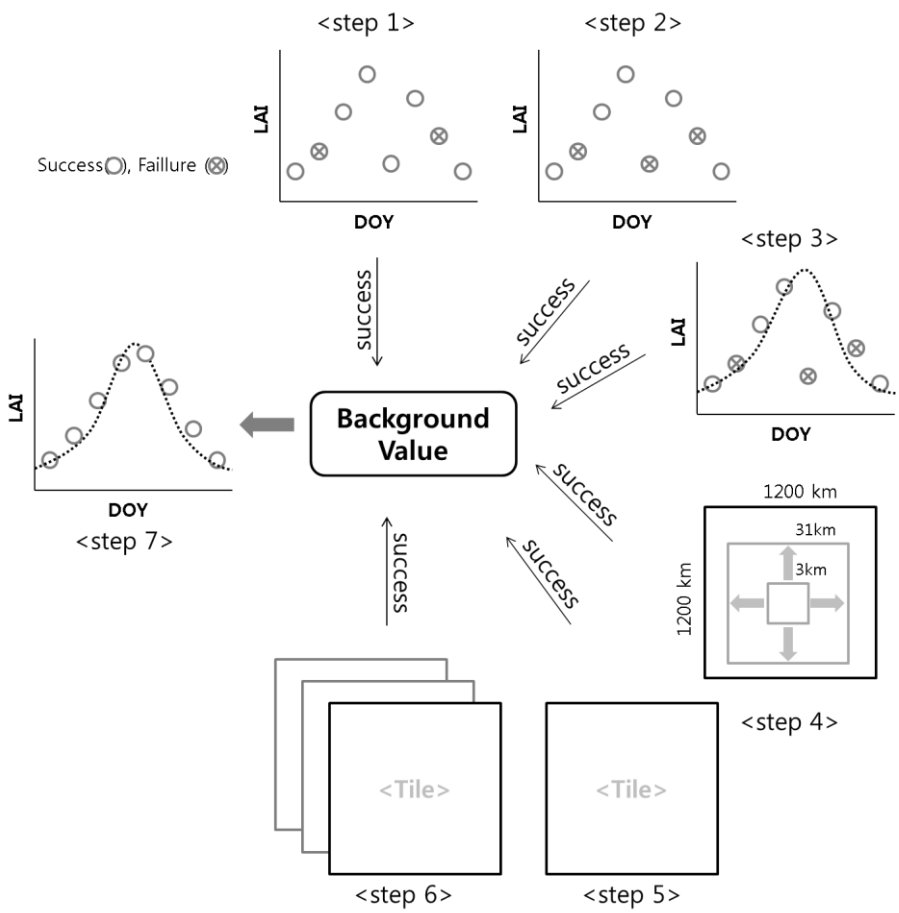

Figure 4 Background value computation scheme. 1 km×1 km stands for one pixel and 1200 km×1200 km stands for one tile of MODIS LAI data.

Step 1. Multi-year mean

Multi-year averages of MODIS LAI data are calculated pixel by pixel. In this calculation, all data which is lower than 50 percent of the overall multi-year maximum is removed. Up-down-up patterns in time series of MODIS LAI tend to be caused by ‘low value’ (less than 50 percent of maximum value of multi-year data) in Step 1. Removing these values could reduce the frequency of up-down-up patterns. Furthermore, calculations of multi-year average are considered successful when the number of data remaining after the removal of ‘low value’ is more than 4. The background values for the 8-day composites are equal on the same DOY of all years.

Step 2. Removing outliers

In order to prevent the frequency of up-down-up patterns, unreasonable drops are removed within a time domain window (half width of window is 6). Since decrease and increase of LAI by half of maximum LAI within 8 to 48 days hardly occur in natural ecosystem, unreasonable drops are defined as values lower than 65 or 40 percent of the average of top three values at both sides and one side, respectively. Only drops are removed for forested areas (EBF, ENF, DBF, DNF) while both drops and

rises are removed for non-forested area. In this process, the number of missing values increases.

Step 3. Temporal gap filling with Savitzky–Golay filters

As temporal gap-filling method, Savitzky–Golay filtering (SG filters, Eq. 3) was used (half width of window *m* is 4 and the degree of polynominal is 2). SG filtering is considered successful when the number of data used in SG filtering is more than 4. Missing values in Step 2 are substituted with the successful values of SG filtering.

$$Y_j=\sum_{i=-m}^{i=m} \frac{1}{2*|m|+1} * Y_{j+i} \qquad \text{(Eq. 3)}$$

Step 4. Local Per Class mean

In this process, spatial moving average is used in each land cover type, based on the result of Step 3. Moving average starts from 3 x 3 (half width: 1) to 31 x 31 (half width *m*: 15) matrix. For matrices smaller than 25 x 25, it is considered successful when the number of data within a matrix is over *m*+2. For larger matrices, the result of moving average replaces missing value when the number of data within a matrix is more than 10.

Step 5. Per Class mean

For the remaining empty pixels after Step 4, the average value of Step 4's results of the same land cover within a tile will substitute for missing values. In most cases, empty pixels do not exist after Step 5 (move to Step 7, figure 5). Otherwise, Step 6 is required to fill the remaining missing value.

Step 6. Multi-year per Class mean

Average values of the same land cover type of all years on the same DOY replaces empty pixels.

Step 7. Temporal smoothing with SG filters

As the final step for background value computation, SG filter is applied to the filled data. In this process, the data smoothened out while maintaining the locations of maximum and minimum value.

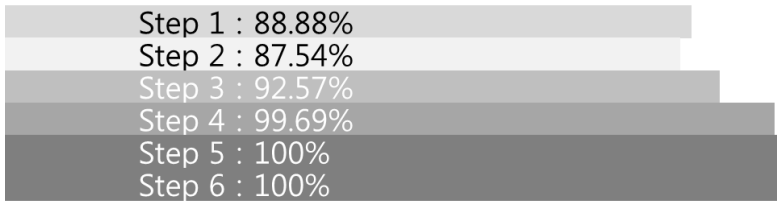

Figure 5 Percent of filled data in the Korean peninsula at each step of background value computation (year : 2009, doy : 113).

⑤ Calculating Observation value.

Step 1. Data filtering

Observation value calculation starts with filtering out data of unsatisfactory quality (QC≠0 and QC≠32) from MODIS LAI products. Unlike Case 1, results of step 1 are different for each year. The remaining data are with QC =0 or QC =32.

Step 2. Removing drops and rises.

Step 2 is the same as case 2 with the exception of the definition of unreasonable drops. In step 2, unreasonable drops are defined as follows:

Definition 1: The values which are lower than 50 and 40 percent of the average of top three values at both sides and one side, respectively.

Definition 2: The values which are lower than 50 percent of the most adjacent values at both sides (half width of window is 6).

Definition 2 was added in observation value calculation since ‘low value’ which can be removed in Step 1 of background value calculation was not removed.

Step 3 to Step 7.

The remaining steps for observation computation (from step 3 to step 7) are the same as those for background value computation (from step 3 to step 7).

2) Change in Land cover type

Land cover type is important in estimating GPP and ET in BESS since several key parameters, such as maximum carboxylation rate (Vcmax) and leaf optical properties, depend on land cover types [*Ryu et al.*, 2011]. MODIS land cover product used in BESS is known to have 75% accuracy [*Friedl et al.*, 2010]. BESS uses MODIS land cover product type 1 (International Geosphere-Biosphere Programme, IGBP). However, MODIS daily LAI algorithm (MOD15A1) uses MODIS Land cover product type 5 (PFT) and MODIS 8 day LAI product (MOD15A2) is based on MOD15A1. Mixed forests (MF) counts for 39.31 percent of MODIS land cover type 1 in tile h28v05 of year 2009 while MODIS land cover type 5 do not have classification of MF. In MODIS land cover type 5, 56.70 percent and 29.24 percent of MF classified in land cover type 1 is in deciduous broadleaf forests (DBF) and evergreen needleleaf forest (ENF), respectively. In BESS, Vcmax of mixed forests in the Korean peninsula is 55 μmol m^{-2} s^{-1} while Vcmax of DBF and ENF is 58 μmol m^{-2} s^{-1} and 32 μmol m^{-2} s^{-1}, respectively. Spatial mismatch between land cover used in BESS and in MODIS LAI product could cause uncertainties in quantification of GPP and ET. This study changes land cover used in BESS from land cover type 1 (IGBP) to land cover type 5 (PFT).

Table 4 Comparison of classifications of MODIS land cover type 1 and type 5 [*Friedl*, n.d.]

Land Cover Type 1	Land Cover Type 5
Evergreen needleleaf forest	Evergreen needleleaf forest
Evergreen broadleaf forest	Evergreen broadleaf forest
Deciduous needleleaf forest	Deciduous needleleaf forest
Deciduous broadleaf forest	Deciduous broadleaf forest
Mixed forests	
Closed shrubland	Shrubs
Open shrublands	
Woody savannas	
Savannas	Savannah
Grasslands	Grass
Permanent wetlands	Cereal crop
Croplands	Broadleaf crops
Urban and built-up	Urban and buit-up
Cropland/natural vegetation mosaic	
Snow and ice	Snow and ice
Barren or sparsely vegetated	Barren or sparsely vegetated

4. Evaluation

1) Evaluation method

To evaluate the results of rTSF and BESS, the systematic error (bias), root-mean-square error (RMSE), systematic RMSE ($RMSE_s$), unsystematic RMSE ($RMSE_u$), proportion of $RMSE_s$ to RMSE ($PRMSE_s$) and proportion of $RMSE_u$ to RMSE ($PRMSE_u$) were calculated.

$$\text{bias} = \frac{1}{n}\sum_{i=1}^{n}(x_s - x_o)$$

$$\text{RMSE} = [\frac{1}{n}\sum_{i=1}^{n}(x_s - x_o)^2]^{1/2}$$

$$\text{RMSE}_s = [\frac{1}{n}\sum_{i=1}^{n}(\hat{x}_s - x_o)^2]^{1/2}$$

$$\text{RMSE}_u = [\frac{1}{n}\sum_{i=1}^{n}(x_s - \hat{x}_s)^2]^{1/2}$$

$$\text{PRMSE}_s = (\text{RMSE}_s)^2/(\text{RMSE})^2$$

$$\text{PRMSE}_u = (\text{RMSE}_u)^2/(\text{RMSE})^2$$

Where x_s and x_o denote the modeled and measured values, respectively. i is i^{th} sample and n is the number of sample used in evaluation. $\hat{x}_s$ is the value of the linear regression of x_s on x_o (i.e. $\hat{x}_s = a * x_o + b$, where a is slope and b is intercept).

Bias indicates a measure of systematic inaccuracy of the model performance and RMSE is the overall measure of the model agreement with field data. Low value of bias and RMSE indicates better performance of model. $RMSE_s$ and $RMSE_u$ are RMSE which arises from systematic and unsystematic errors, respectively ($RMSE^2 = RMSE_s^2 + RMSE_u^2$) [*Willmott*, 1982]. $PRMSE_s$ and $PRMSE_u$ measure the proportion of the total RMSE induced by systematic and unsystematic biases, respectively.

The errors of MODIS geolocation become larger as the sensor field of view increases but the error is reduced to 50 m at nadir [Wolfe, 2002]. For this reason, evaluation studies have been recommended to use the mean value of surrounding pixels (mostly, 3 km x 3 km) [*Tan et al.*, 2006; *Verger et al.*, 2011]. However, it is hard to find a truly homogeneous 3 km x 3 km area and using 3 km x 3 km pixels could induce more uncertainties [*Fang et al.*, 2008]. At heterogeneous sites, single pixels could be better for evaluation [*Fang et al.*, 2008]. Field measurement sites, used in this study, are not homogeneous 3 km x 3 km areas. Therefore, the simulated results were evaluated at the 1 km x1 km pixel enclosing the sites where field measurements were conducted.

2) Evaluation data

To evaluate the result of rTSF, field measurements of LAI were used. LAI

measurements have been carried out using LI-2000 (http://www.licor.com), from 2006 to 2011 at GCK and GDK.

GPP from BESS was evaluated using eddy-covariance data of GCK, GDK and Haenam farmland (HFK). GPP data from eddy-covariance system is the sum of NEE and ecosystem respiration. Eddy covariance derived GPP data are available from 2007 to 2010 at GCK and GDK, 2006 and 2008 at HFK. Values of GPP at Mt. Changbai published in *Zhang et al.* [2006a] and *Zhang et al.* [2006b] were used in the evaluation.

ET was evaluated with two data streams: ET data from eddy-covariance system and from water balance at basin scale. Eddy-covariance ET data can be used to evaluate a single pixel on a daily basis while the annual ET from BESS at basin scale can be compared with water balance derived ET.

III. Results

1. Evaluation

1) Reprocessing MODIS LAI product

The results of rTSF, raw MODIS, mTSF and BESS were compared to ground measurement in GDK site (Figure 6). Raw MODIS data shows the largest discrepancy with *in-situ* data (RMSE of rTSF: 1.13, raw MODIS: 1.45, mTSF: 1.37 and BESS: 1.22). LAI values from rTSF, raw MODIS, mTSF and BESS are negatively biased by -0.46, -0.85,-0.85 and -0.50, respectively. RMSE of results from the four methods are induced mainly from unsystematic errors (PRMSEu of rTSF: 0.83, raw MODIS: 0.70, mTSF: 0.49 and BESS: 0.80). Difference between field measurement LAI and the result of the rTSF showed a statistically significant improvement compared to difference between field measurement LAI and the result of raw MODIS and BESS (Table 5).

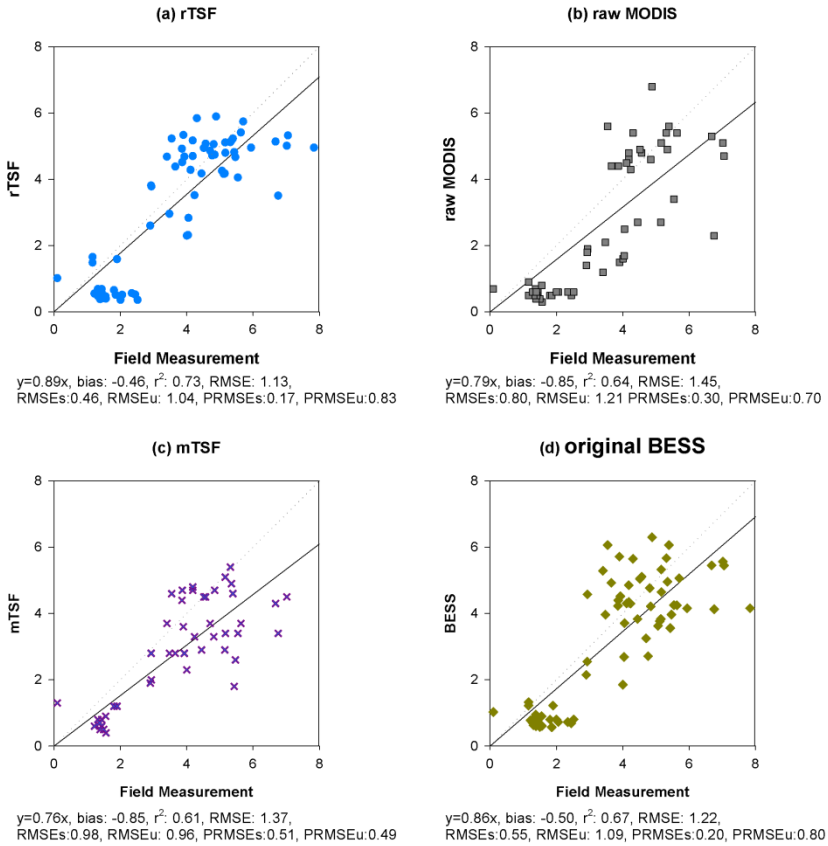

Figure 6 Comparison of LAI from (a) rTSF, (b) raw MODIS (QC=0 or QC=32), (c) mTSF and (d) original BESS, and field measurement LAI. Field measurement is conducted at Gwangneung deciduous forest. The dotted line is 1:1 line and the solid line is the regression line.

Table 5 P-values for t-test on difference between results of rTSF - field measurement LAI and raw MODIS - field measurement LAI (raw MODIS), mTSF - field measurement LAI (mTSF) and BESS - field measurement LAI (BESS).

	raw MODIS	mTSF	BESS
p-value	0.0264	0.1767	0.0009

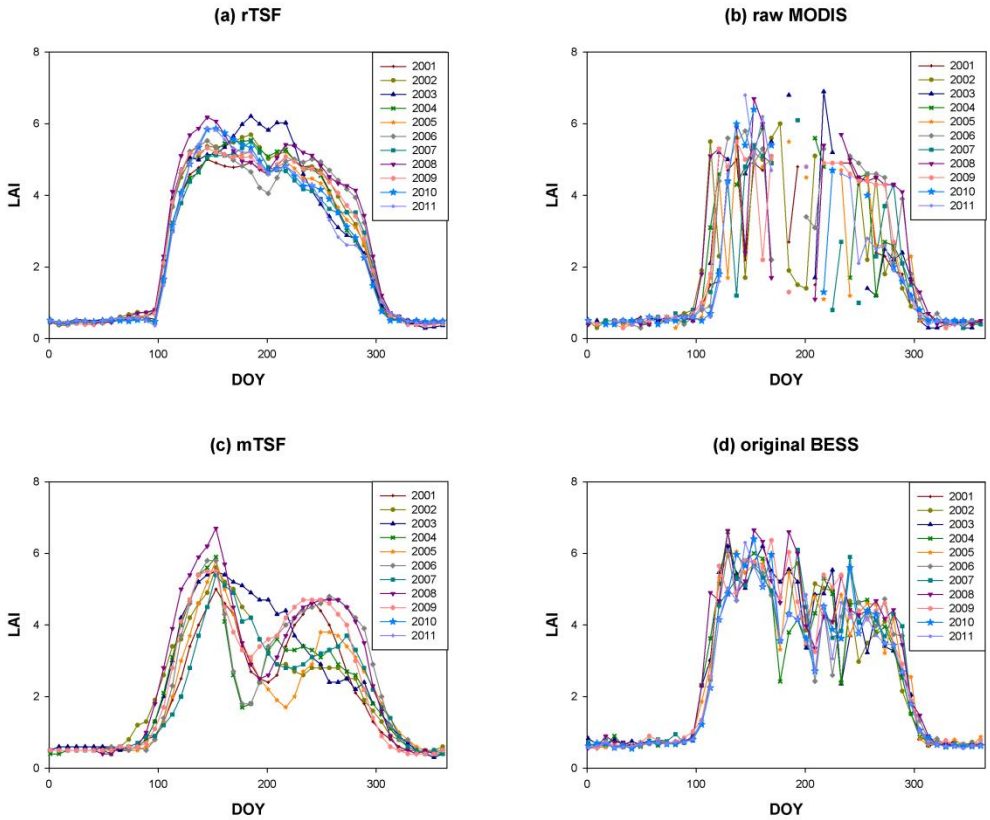

Figure 7 Time-series of multi-year LAI values of (a) rTSF, (b) raw MODIS (QC=0 or QC=32), (c) mTSF and (d) original BESS at Gwangneung deciduous forest.

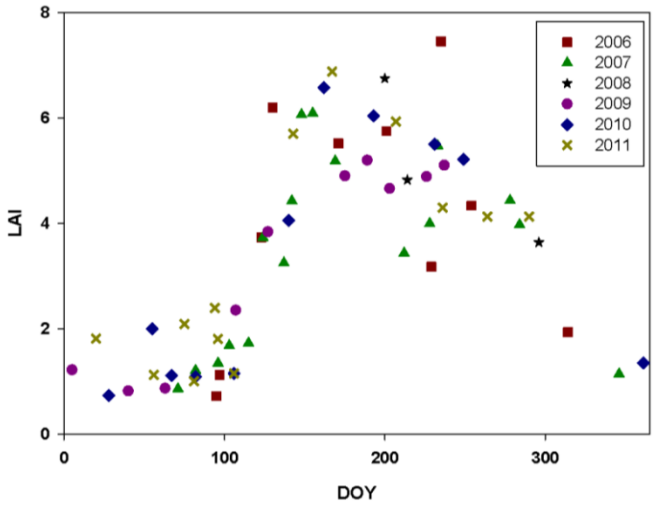

Figure 8 Seasonal to interannual patterns of LAI measured at Gwangneung deciduous forest.

Figure 7 shows time-series of multi-year LAI values of rTSF, raw MODIS, mTSF and BESS at GDK. LAI derived from raw MODIS and BESS have much noise which led the inter-annual variations of MODIS and BESS derived LAI to be vague. LAI from mTSF has up-down-up patterns in all years that barely appear in field measurement (Figure 8). Interannual variation is shown in rTSF derived LAI and small up-down-up pattern of rTSF LAI is found in 2006.

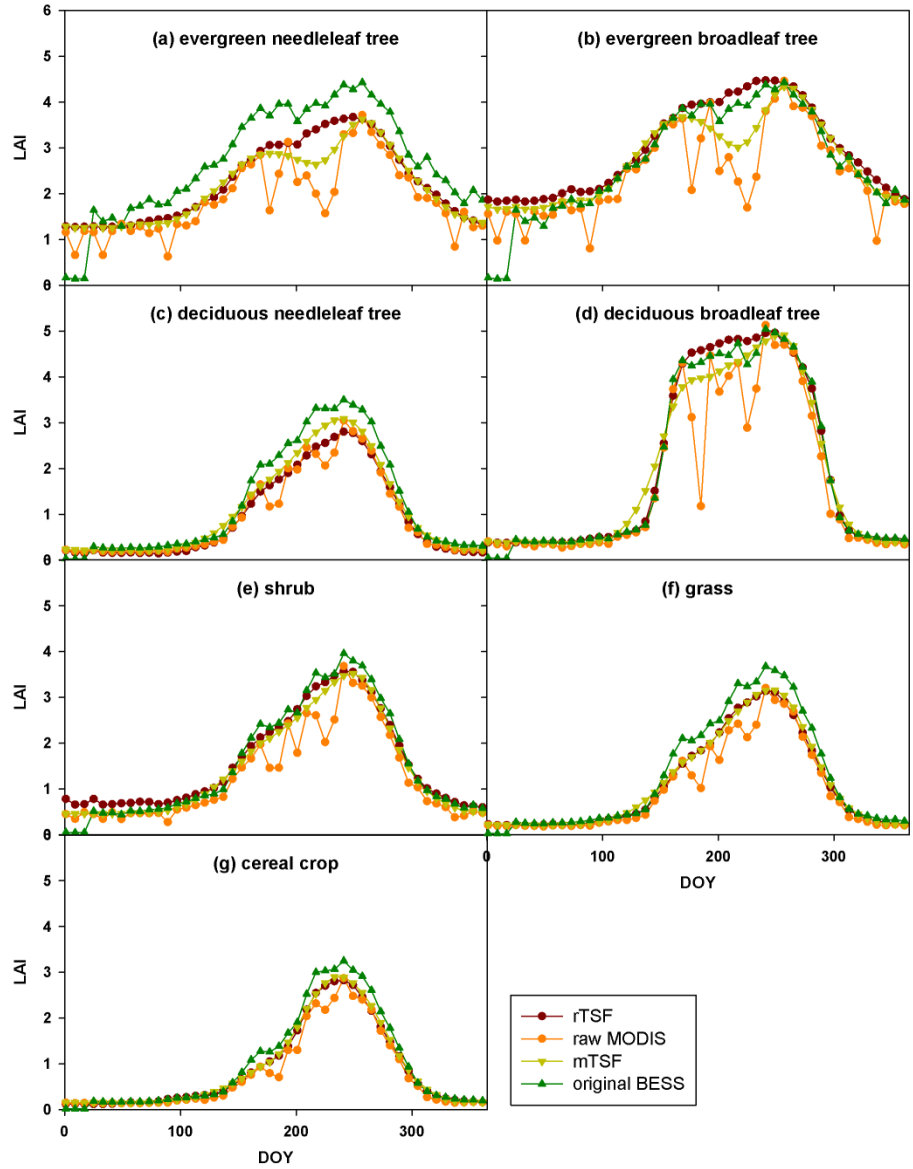

Figure 9 Time series plots of means of rTSF, raw MODIS, mTSF and BESS derived LAI for each plant functional type from in the Korean Peninsula (year 2009)

Figure 9 shows temporal patterns of averages of LAI from four different LAI products for each plant functional type (PFT) in the Korean Peninsula for the year 2009. Overall, four different LAI products have similar temporal patterns for LAI in different PFT. However, BESS derived LAI tends to have larger LAI values for most PFT and raw MODIS LAI has noise, which is severe in forested area, during summer time. LAI from mTSF has up-down-up patterns in Evergreen Broadleaf forest and Evergreen Needleleaf forest (Figure 9 (a) and (b)). Temporal patterns of rTSF derived LAI are smoother, compared to those of other LAI products and do not have up-down-up patterns in all PFT.

Better estimates of LAI will improve the performance of models for carbon and water exchange between the atmosphere and the land [Asner et al., 2003]. LAI from rTSF seems to better reflect phenology of LAI; frequency of up-down-up patterns is lower than that of mTSF derived LAI and the noise is much less than those of raw MODIS and BESS derived LAI. LAI from rTSF can be used effectively for quantification of GPP and ET in BESS.

2) BESS derived GPP and ET

① Evaluation with field measurement

The BESS derived daily ET and GPP was evaluated with flux tower

data. BESS shows strong correlation for GPP at GDK (r^2=0.802) and ET at GDK, GCK, HFK and SMK (r^2= 0.840, 0.832, 0.727 and 0.711, respectively). The BESS derived monthly GPP also shows very strong relation with the flux tower GPP at Mt. Changbai in China (r^2 = 0.9503, Figure 12). GPP at GDK and GCK are positively biased (0.996 for GDK and 0.048 for GCK), with overestimates from BESS (Figure 10) while GPP at HFK and Mt. Changbai show negative bias (-1.080, -21.3931), with underestimated GPP from BESS (Figure 10 and 12). GPP from flux tower data at GDK, GCK, and HFK in winter show high value (2 – 4 gC m^{-2} day^{-1}) compared to GPP from BESS (~0 gC m^{-2} day^{-1}).

BESS derived ET at GDK, GCK and SMK are overestimated, compared to flux tower ET (bias = 0.522, 0.272 and 0.131, respectively) while BESS derived ET at HFK and CFK are negatively biased (bias = -0.190 and -0.293). RMSE for GPP at HFK is mostly derived from unsystematic errors and RMSE for ET at most of sites (except GDK) are mostly derived from unsystematic errors.

Solar irradiance of BESS is correlated with flux tower measurement (r^2 = 0.746, Figure 13). Daily solar irradiance of BESS has higher value than that of flux tower (bias = 2.021). 79.6% of RMSE for solar irradiance arises from unsystematic errors.

‘

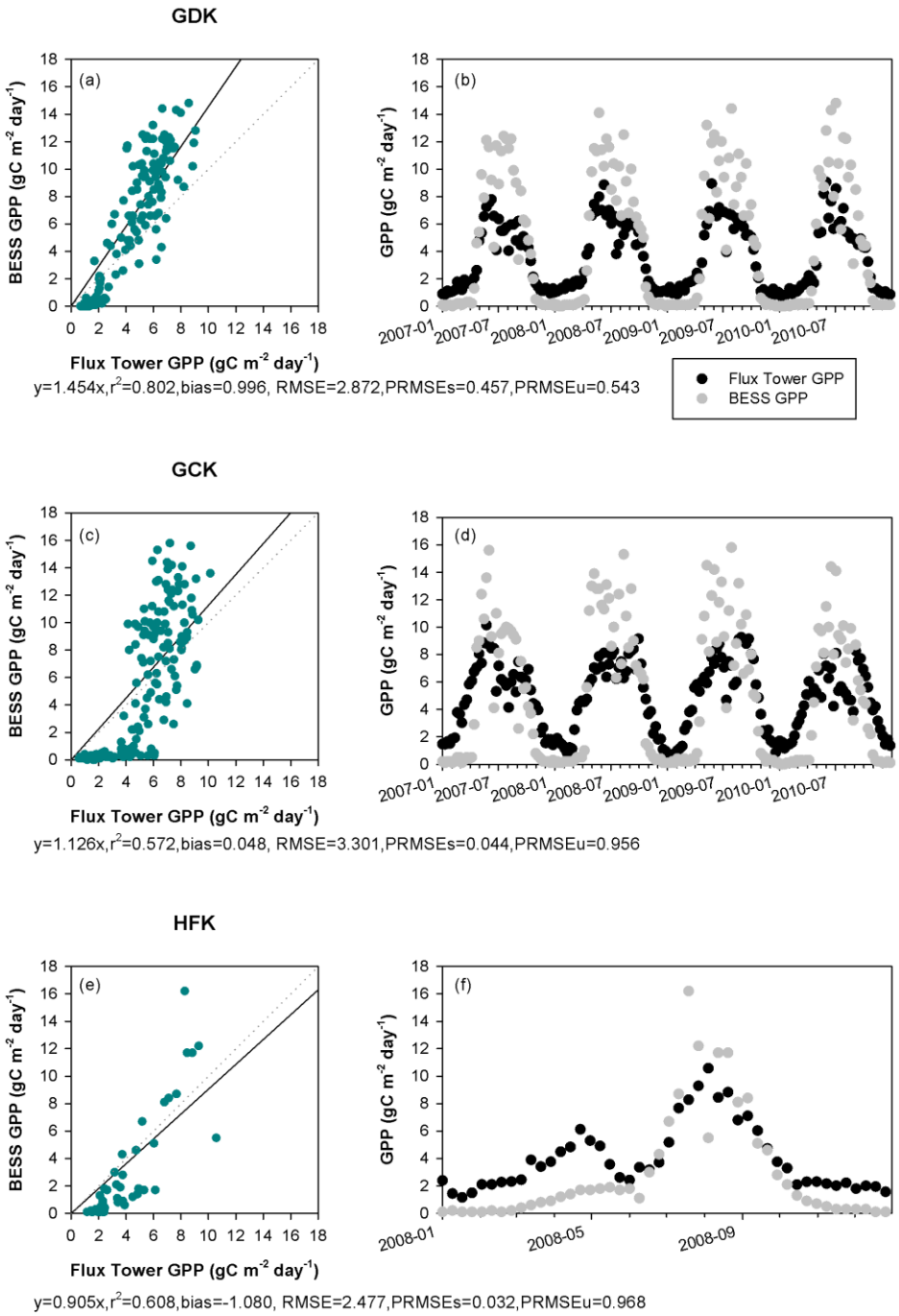

Figure 10 Scatter plots of daily gross primary productivities from flux tower measurement and BESS at (a) GDK, (c) GCK and (e) HFK. Time-series plots of daily gross primary productivities from flux tower measurement and BESS at (b) GDK, (d) GCK and (f) HFK. The dotted line is 1:1 line and the

solid line is the regression line.

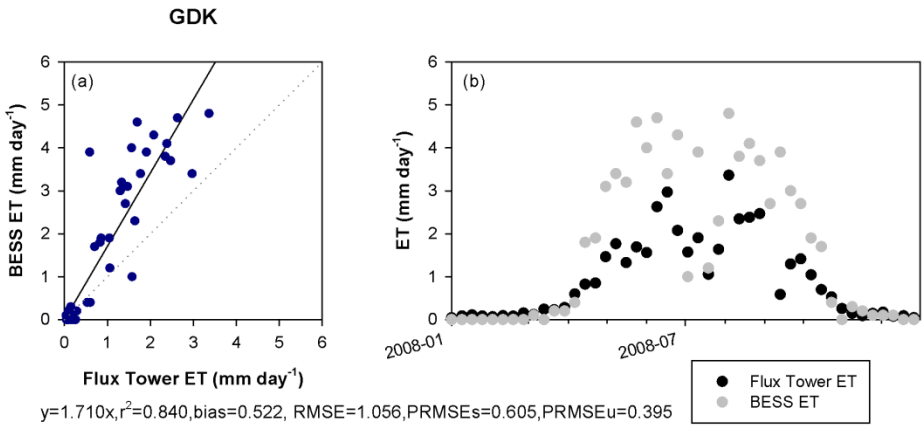

y=1.710x,r^2=0.840,bias=0.522, RMSE=1.056,PRMSEs=0.605,PRMSEu=0.395

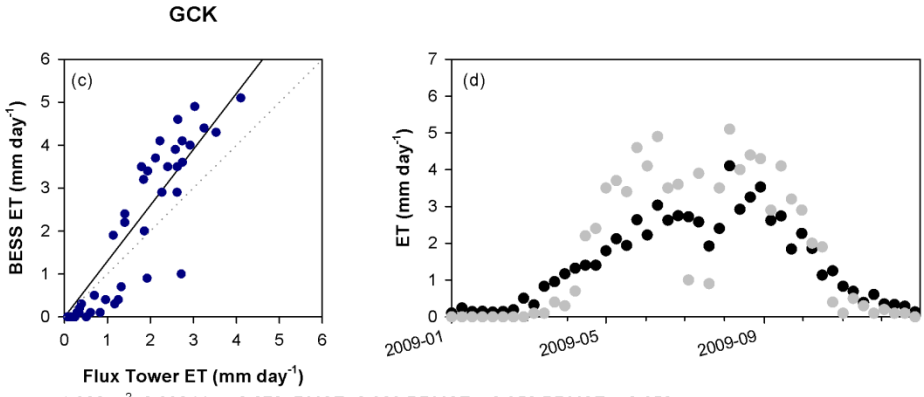

y=1.302x,r^2=0.832,bias=0.272, RMSE=0.903,PRMSEs=0.350,PRMSEu=0.650

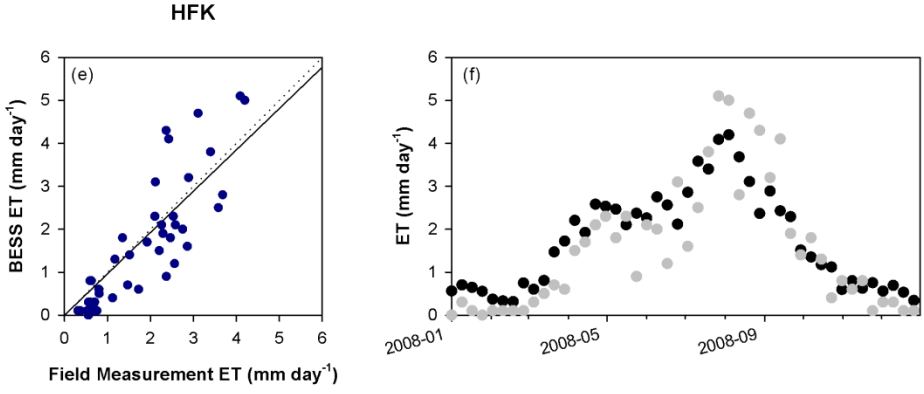

y=0.962x,r^2=0.727,bias=-0.190, RMSE=0.766,PRMSEs=0.011,PRMSEu=0.989

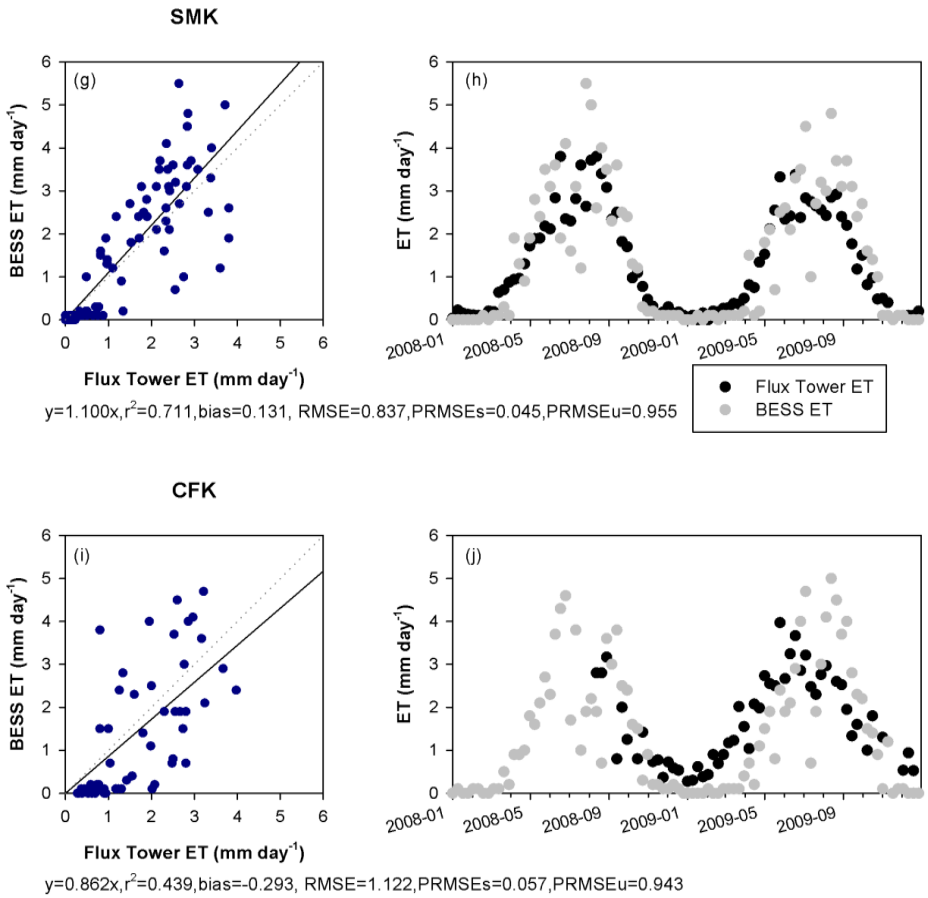

Figure 11 Scatter plots of daily evapotranspiration from flux tower measurement and BESS at (a) GDK, (c) GCK, (e) HFK, (g) SMK and (i) CFK. Time-series plots of daily evapotranspiration from flux tower measurement and BESS at (b) GDK, (d) GCK, (f) HFK, (h) SMK and (j) CFK. The dotted line is 1:1 line and the solid line is the regression line.

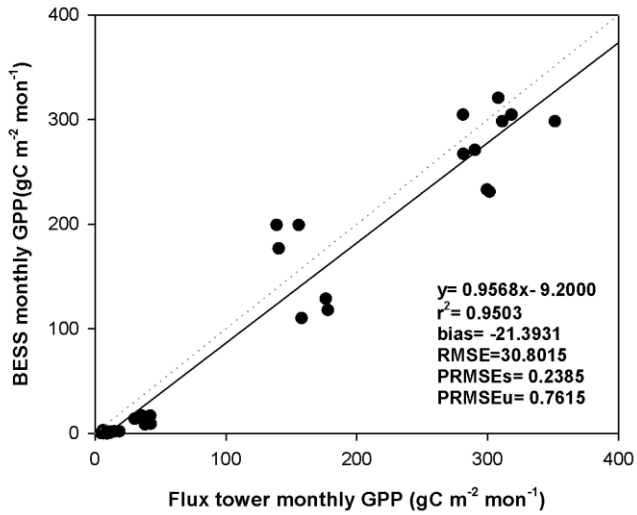

Figure 12 Scatter plot of monthly gross primary productivities at Mt. Changbai between flux tower measurement (derived from [*Zhang et al.*, 2006a; *Zhang et al.*, 2006b]) and BESS. The dotted line is 1:1 line and the solid line is the regression line.

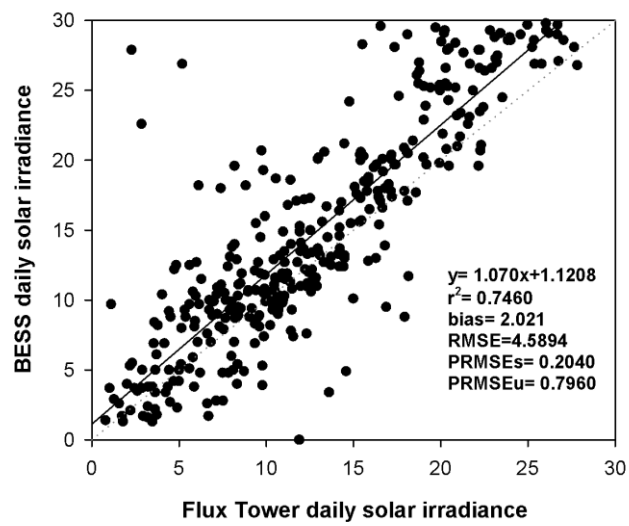

Figure 13 Scatter plot between flux tower daily solar irradiance and BESS daily solar irradiance at GDK. The dotted line is 1:1 line and the solid line is the regression line.

② Evaluation with water balance derived ET

BESS-derived ET was compared to water balance derived ET at basin scale (Figure 14). Annual precipitation and discharge data within basins were required in calculation of water-balance derived ET. Basin scale annual precipitation was estimated by using a precipitation map. Precipitation map was produced annually by using spatial interpolation of annual precipitation data provided by Korea Meteorological Administration (www.kma.go.kr). Discharge data were obtained from Water Management Information System (www.wamis.go.kr). Data of small and medium sized basin, which are located on upstream, were used in evaluation of ET from BESS. Basins with any big dam on their upstream were excluded since dams prevent natural stream flows. Also, large sized basins such as Han

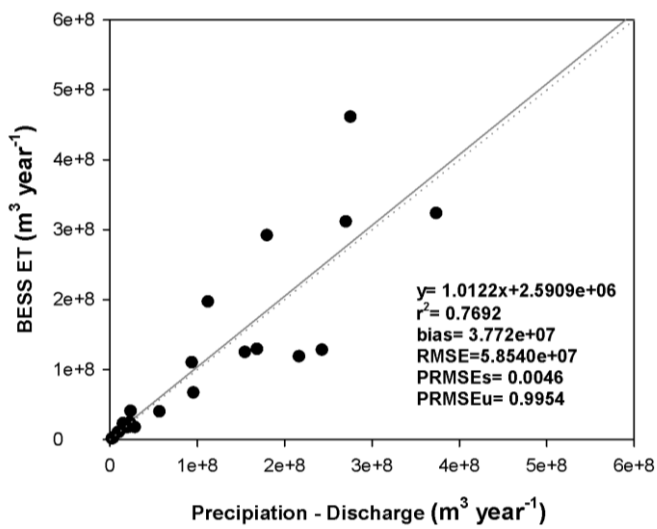

Figure 14 Comparison of evaporation between the water-balance derived evaporation from basins and BESS.

River and Nak-Dong River were used. Data points with excess or low (less than 10% of percipitation) discharge to precipitation are excluded. The basin scale ET was calculated using a water-balance approach (rainfall minus discharge) as reported by *Jung et al.* [2010]. Annual ET for 20 basins was used in evaluation of BESS derived annual ET. BESS derived basin scale ET is strongly correlated with water-balance approached ET and has low negative bias (r^2 of 0.77 and bias of -3.78 e+07)

2. Analysis on Spatial and Temporal patterns

1) Annual GPP and ET

The mean annual land GPP over the eleven years (2001-2011) is 1183 gC m^{-2} $year^{-1}$ (equivalent to 0.29 PgC) throughout the Korean Peninsula with relative standard deviation (STD) of 2.44 % and the mean annual land ET is 491 mm $year^{-1}$ (equivalent to 125.28 km^3 $year^{-1}$) with higher interannual variation (relative STD of 3.27 %, Figure 15), compared to GPP. GPP and ET are higher in South Korea compared to those in North Korea. Land cover change, defined as changes in MODIS land cover type of each pixel during the eleven years (2001-2011), causes higher relative STD (Table 5). Relative STD of GPP is higher in crop land compared to that in forest (Table 6) while that of ET is lower in crop land.

Low precipitations (less than 75% of mean precipitation during the years of 2001 through 2011) were recorded in 2001 and 2008. The sensitivity of ET to the stomata conductance during growing season (Mar - Nov) was averaged. The sensitivity of ET in winter was excluded since ET in winter is very low compared to the other season (Figure 18). The sensitivity of ET to the stomata conductance in dry years is highly positive in high mountain areas (>0.8) while the other areas show similar sensitivity value with the one in non-dry years.

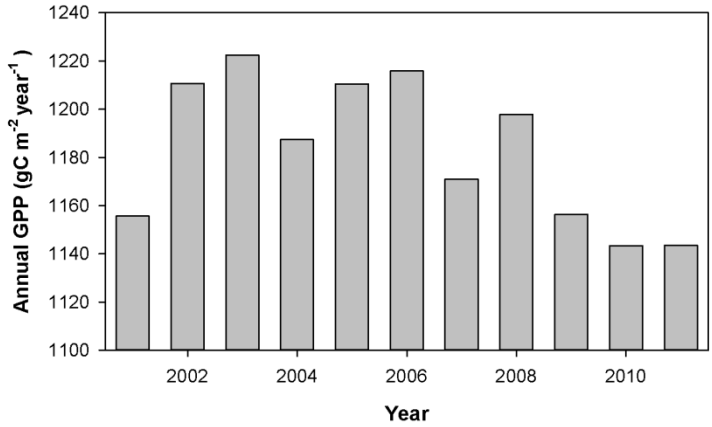

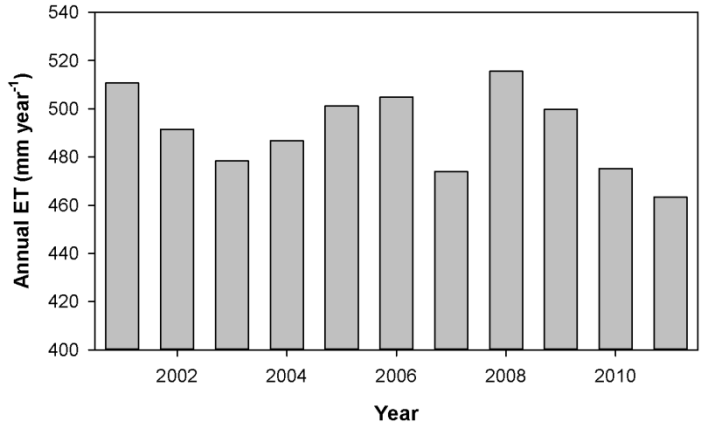

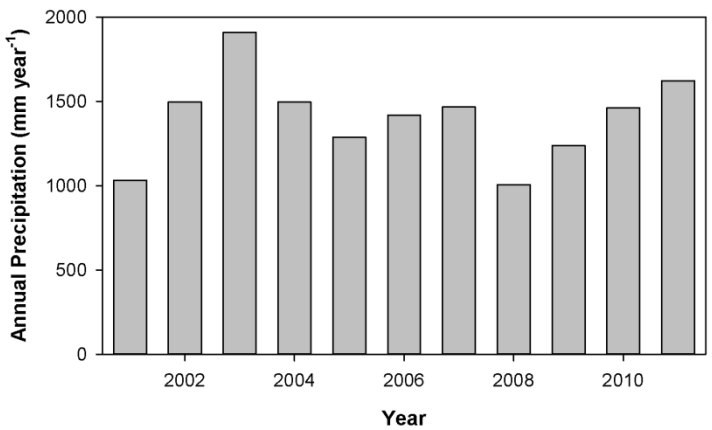

Figure 15 Annual (a) gross primary productivity, (b) evapotranspiration and (c) precipitation from 2001 to 2011.

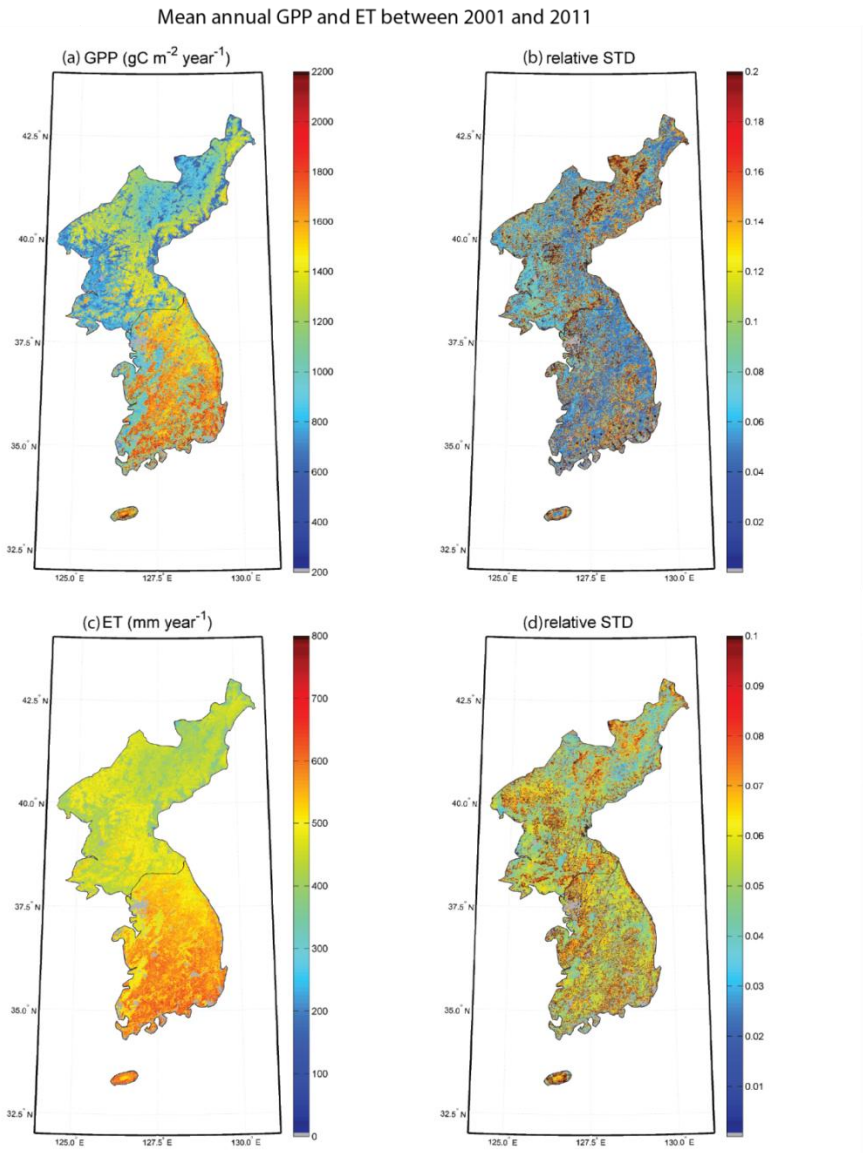

Figure 16 Maps of mean annual (a) gross primary productivity and (c) evapotranspiration. Maps of relative standard deviation of (b) gross primary productivity and (d) evapotranspiration. Grey area indicates urban.

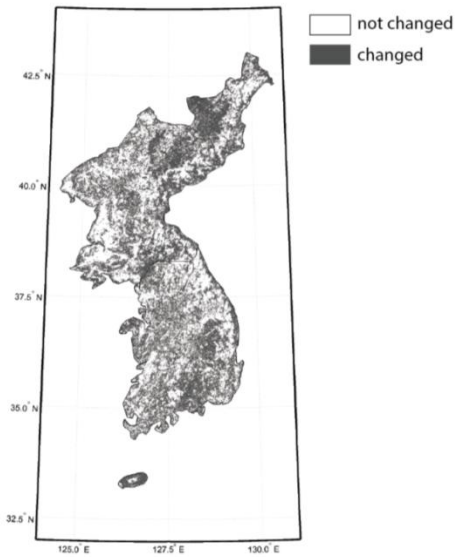

Figure 17 Map of land cover change. White indicates that land cover did not change during the years of 2001 through 2011 and black indicates that land cover changed.

Table 6 Averages of ET and GPP relative standard deviation under land cover changed and not changed

	Land cover changed	Land cover not changed
GPP	0.2963	0.2226
ET	0.107	0.055

Table 7 Averages of relative standard deviation of GPP and ET in forest and crop of which land cover has been not changed over eleven years (2001-2011).

	GPP	ET
Forest	0.1671	0.0607
Crop	0.2486	0.0514

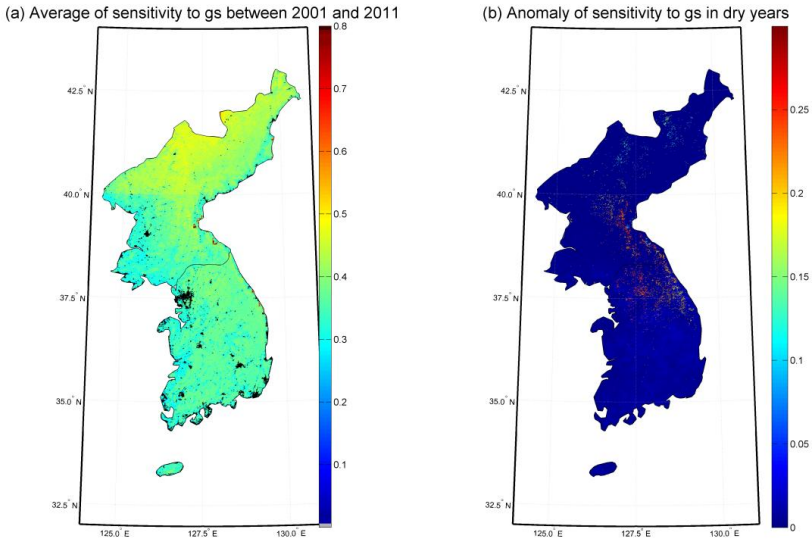

Figure 18 Map of the averaged sensitivity of evapotranspiration to canopy conductance (gs) through 2001 to 2011 (a). Map of anomaly of sensitivity of evapotranspiration to gs in dry year 2001 and 2008. The sensitivities of evapotranspiration to the canopy conductance during the growing season (Mar to Nov) are only taken into account. Black area indicates urban.

2) Seasonal GPP and ET

Most of GPP and ET in the Korean Peninsula occur in summer (62.93% and 44.45%, respectively, Table 7). GPP in 2001 is lowest of the eleven years (2001-2011). Precipitation in 2001 and 2008 are very low (Figure 15), and the phenomena of low precipitation occurred in spring of 2001 and autumn of 2008 (Figure 19). The Korean Peninsula experiences dry season in spring and autumn (Figure 22). The proportion of GPP contributed from sunlit is higher in spring and winter than that from shaded leaves while GPP occurred in shaded leaves is larger than that in sunlit in summer.

ET in spring and autumn are the most sensitive to the canopy conductance while in summer ET is sensitive to both canopy conductance and available energy (Figure 21a and 21b). Aerodynamic conductance controls spring ET in northern part of the Korean Peninsula.

Table 8 Seasonal average and relative standard deviation of gross primary productivity, evapotranspiration and precipitation. (Spring: Mar-May, Summer: Jun-Aug, Autumn: Sep-Nov, and Winter: Jan-Feb and Dec)

	GPP ($gC\ m^{-2}\ 3months^{-1}$)		ET ($mm\ 3months^{-1}$)		Precipitation ($mm\ 3months^{-1}$)	
	average	Relative STD (%)	average	Relative STD (%)	average	Relative STD (%)
Spring	185.37	7.91	98.09	7.38	106.84	32.03
Summer	654.41	3.51	224.98	3.39	350.77	17.52
Autumn	192.58	4.65	165.88	4.91	106.96	41.37
Winter	7.46	17.47	17.22	31.49	37.14	

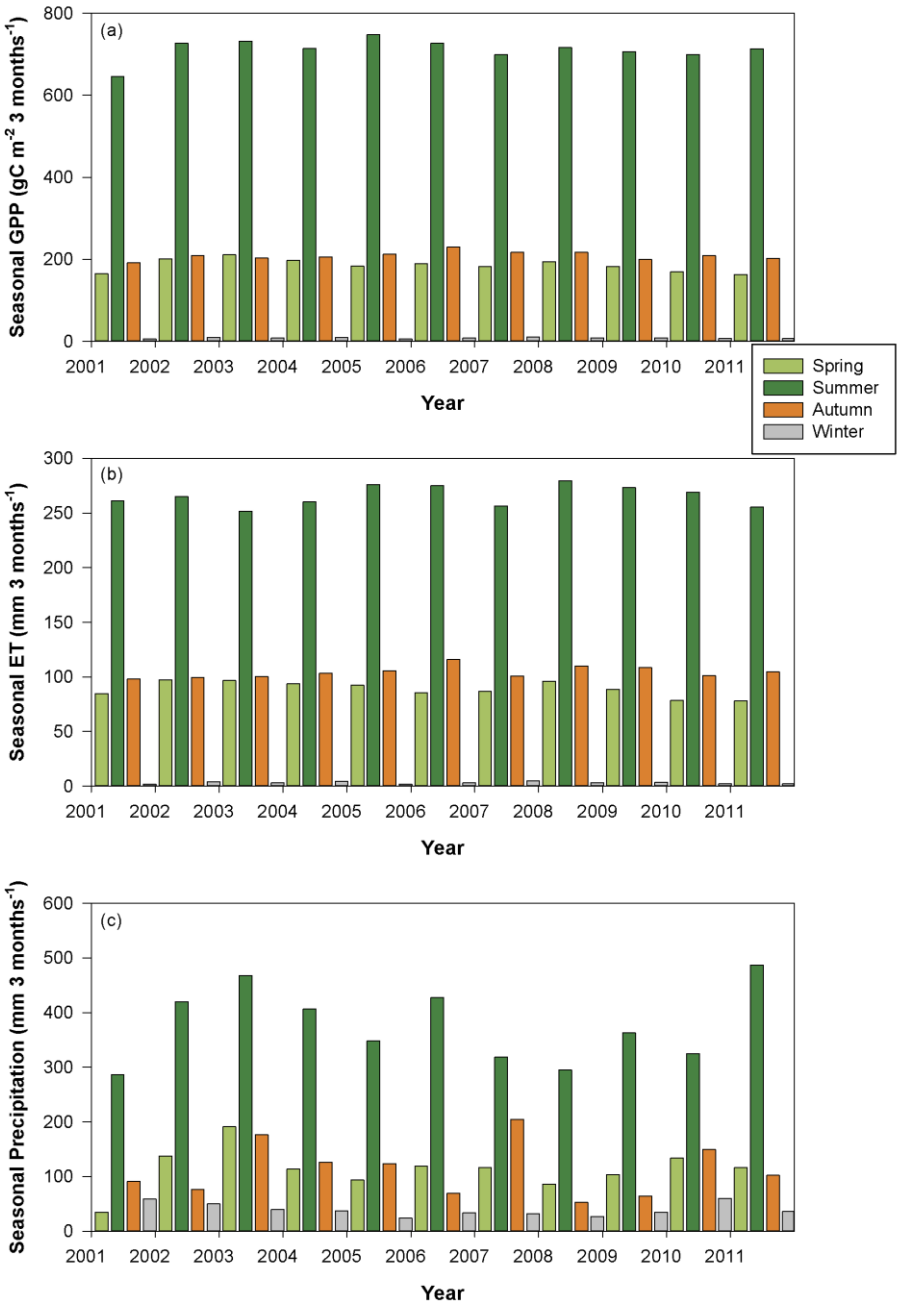

Figure 19 The mean seasonal (a) gross primary productivity, (b) evapotranspiration and (c) precipitation from 2001 to 2011.

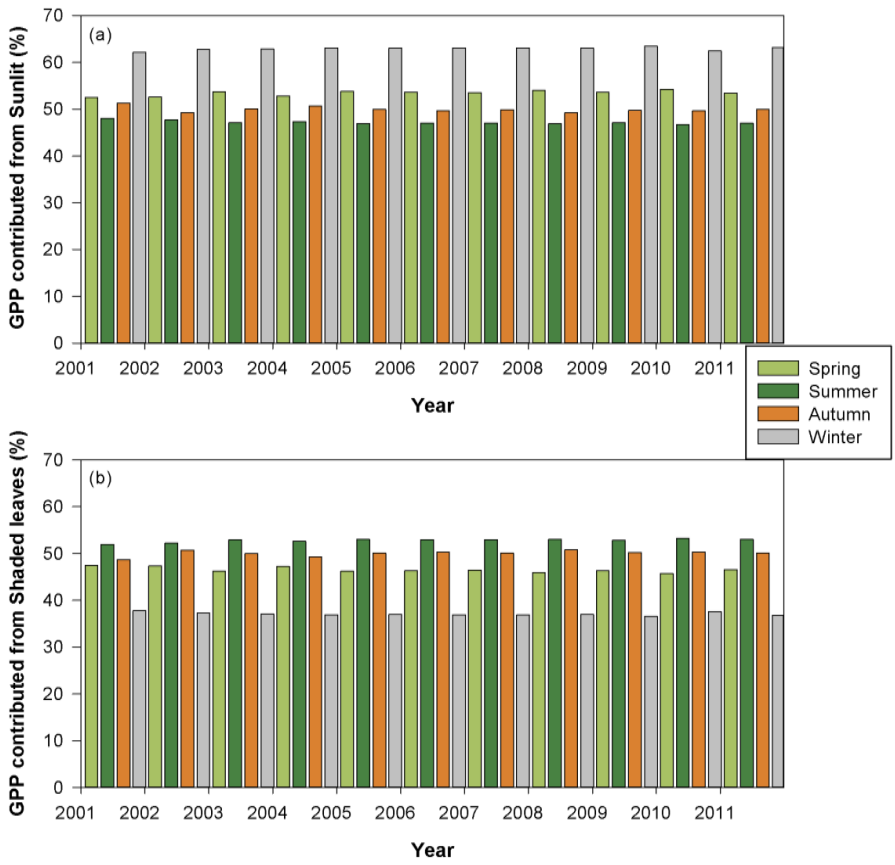

Figure 20 The proportion of seasonal GPP contributed from (a) sunlit and (b) shaded leaves.

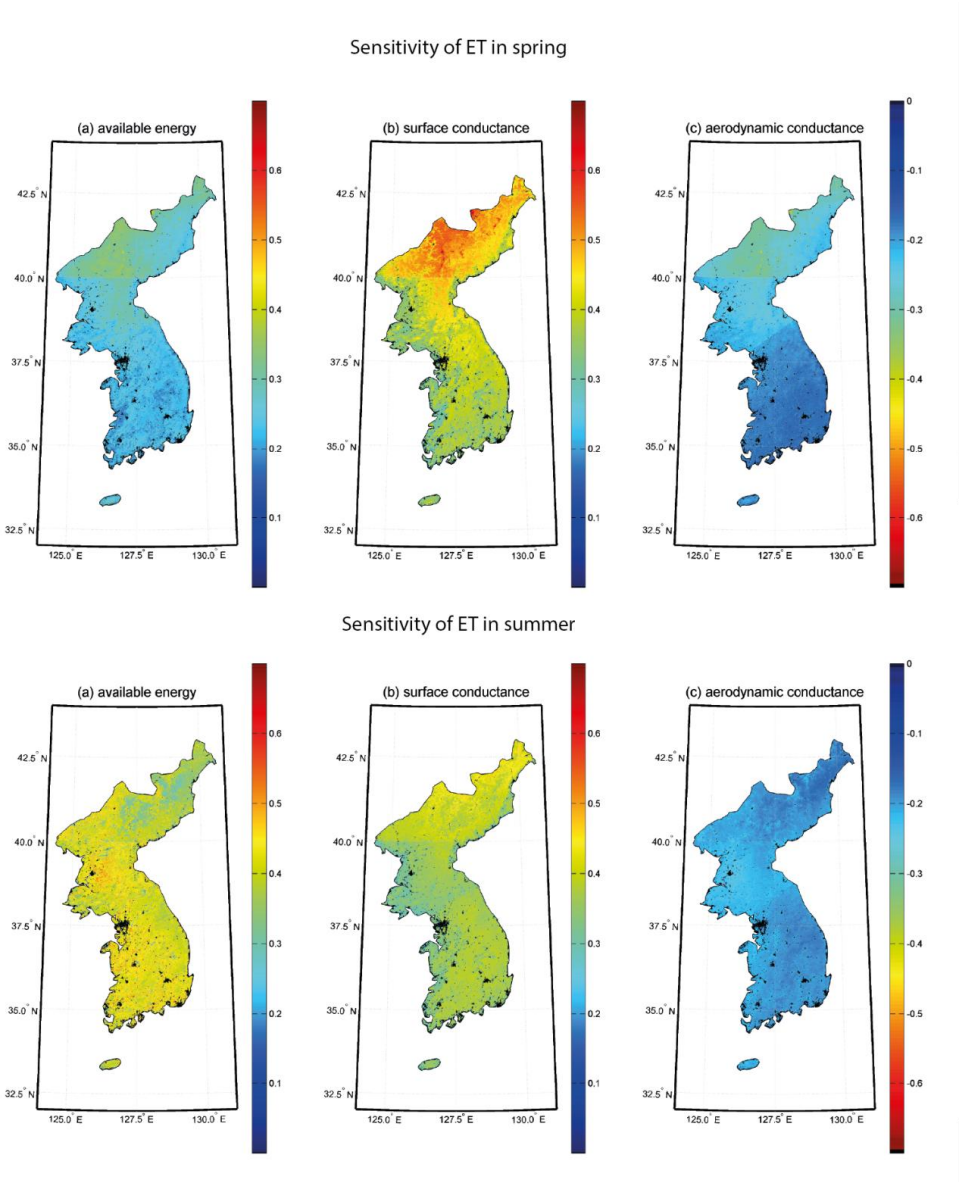

Figure 21a Maps of relative sensitivity of seasonal evapotranspiration to available energy ((a) for spring, (d) for summer and (g) for autumn), canopy conductance ((b) for spring, (e) for summer and (h) for autumn) and aerodynamic conductance ((c) for spring, (f) for summer and (i) for autumn).

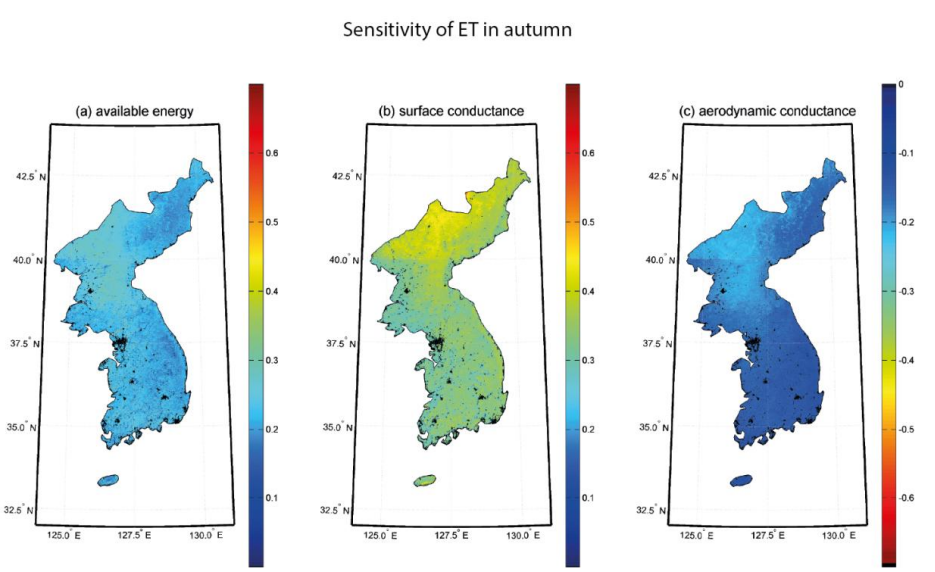

Figure 21b Maps of relative sensitivity of seasonal evapotranspiration to available energy ((a) for spring, (d) for summer and (g) for autumn), canopy conductance ((b) for spring, (e) for summer and (h) for autumn) and aerodynamic conductance ((c) for spring, (f) for summer and (i) for autumn).

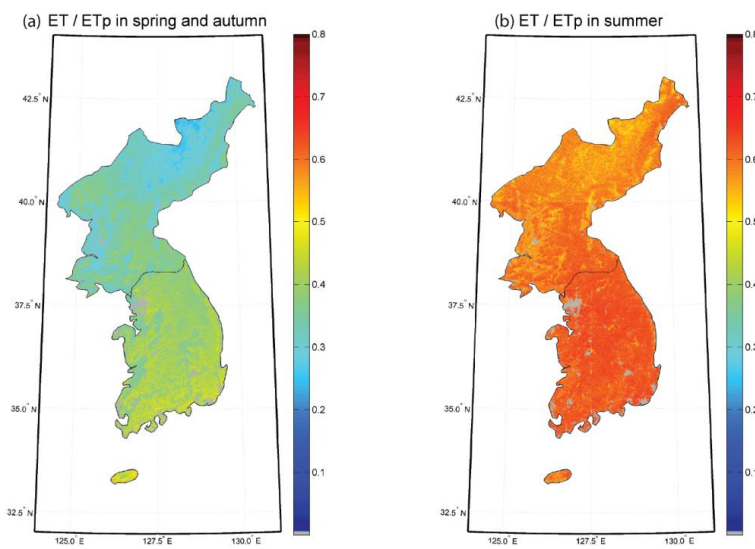

Figure 22 Maps of evapotranspiration / potential evapotranspiration (a) in spring and autumn and (b) in summer.

IV. Discussion

1. Evaluation of BESS.

The performance of BESS in the Korean Peninsula has proven to be reliable when checked against flux tower estimates at HFK, SMK and CFK, data-driven products and basin water balance derived ET (Figure 12 and 13). The correlations between GPP and ET of BESS, and GPP and ET of other data streams are strong. However, GPP and ET of BESS are overestimated compared to flux tower GPP and ET at GDK and GCK. This is partly because solar irradiance, used in BESS as an input variable, is over-estimated compared to that of flux tower (Figure 13). GPP at GCK shows a weak correlation between BESS and flux tower (r^2=0.572). It is thought to be because GCK site, coniferous forest, does not cover a MODIS pixel (1km x 1km) and land cover used in BESS classified a pixel enclosing GCK as DBF, not ENF and high GPP value of flux tower in winter is another reason for the weak correlation. BESS shows a better agreement with large-scale data and monthly data, compared to the agreement with pixel by pixel daily data.

2. Spatial and Temporal Patterns of GPP and ET

North Korea shows lower GPP and ET value than South Korea. Cooler

climate of North Korea could be one reason. It also seems to be due to forest degradation in North Korea. According to Korea Forestry Service (www.forest.go.kr), forests in North Korea have been degraded due to excessive logging and over-exploitation of forest resources.

Interannual variation in GPP and ET is larger in the place where land cover has been changed over the eleven years (2001-2011, Table 6), so that land cover change is thought to be one of major causes of interannual variation in GPP and ET. Crop land shows large interannual variation in GPP and less interannual variation in ET, compared to forest (Table 7). Crop land is largely affected by human activities while forest is not. Large interannual variations of GPP in crop land could mean that agricultural activities have been not constant. ET shows lower interannual variation in crop land than GPP does. Rice paddy accounts for 60.37% of crop land in South Korea between 2002 and 2011 (Statistics Korea, www.kostat.go.kr). Rice paddy contains water during growing season. Regardless of whether there are plants or not, evaporation occurs from the surface of free water. This means that even when agricultural activities do not take place, ET continues to occur while GPP does not.

Drought in spring affects plants' activity throughout the year. In 2001, precipitation during the spring is very low compared to in other years. Low precipitation in leaf-on season could disturb plant growing such as LAI

[*Dong et al.*, 2011; *Kim et al.*, 2010]. As a result, low level of photosynthesis lasts over a leaf life span, so that annual GPP was lower in 2001, compared to the mean annual GPP of the other years.

3. What controls evapotranspiration in Korea?

Biological factor such as canopy conductance has a dominant control over spring and autumn ET in Korea. Spring and autumn, when precipitations are low, are dry season in the Korean Peninsula and soil moisture is expected to be lower in dry season than in non-dry season. Canopy conductance varies along soil moisture gradient [*Alder et al.*, 1996]. Lower soil moisture makes canopy conductance low which causes a high sensitivity of ET to canopy conductance. In summer, the available energy and canopy conductance control ET. The Korean Peninsula experiences summer monsoon when there are lots of clouds in the sky. Clouds prevent solar radiation from reaching the land. Reduced available energy strongly limits ET in summer. Both biological and environmental factors control summer ET in the Korean Peninsula.

ET of dry year in highland is mainly controlled by biological factor. Canopy conductance is highly limited in dry condition [*Alder et al.*, 1996]. Stomata, through which CO_2 and H_2O exchange, is highly affected by soil moisture [*Khatun et al.*, 2011]. Precipitation in high mountain area tends to

flow into lowland and soils at high altitude tend to contain lower moisture [*Qiu et al.*, 2001]. In dry season, the negative relation between elevation and soil moisture content enhances [*Qiu et al.*, 2001]. ET of dry period in highland becomes highly sensitive to the canopy conductance due to low soil moisture contents (Figure 18). However, the other areas show similar values of the sensitivity of ET to the canopy conductance with the averaged sensitivity between 2001 and 2011. According to Korea Soil Information System (www.soil.rda.go.kr), the fine sandy loam is the most common soil texture in the Korean Peninsula (44.2% of fine sandy loam). Fine sandy loam is medium textured soil of which water holding capacity and available water for plants are high [*Brady and Weil*, 2008]. Therefore, soil moisture contents in lowland are expected to be relatively stable even in dry season which means drought does not severely affect plant growing in lowland and its canopy conductance.

4. How do the contributions of sunlit and shaded leaves to GPP change in different season?

Korea's forests are dense in summer, so the proportion of shaded leave is not negligible. The contributions of sunlit and shaded leaves to GPP change with the seasons [*Wittig et al.*, 2005]. In spring and autumn, LAI is low and direct solar radiation reaches most of leaves, so that the contribution of sunlit is larger than that of shaded leaves. However, in summer when LAI is

high, the proportion of leaves getting direct solar radiation is reduced. Instead, the contribution of diffused radiation, reaching shaded leaves, to GPP becomes larger.

Big leaf model does not take shaded leaves into account. According to *Sprintsin et al.* [2012], shaded leaves contribute about 51% to GPP and exclusion of shaded leaves in estimating GPP causes underestimation. Contribution of shaded leaves in the Korean Peninsula is from 40% to 60% during the growing season. Therefore, estimating GPP of the Korean Peninsula by using big leaf model could lead to underestimation.

V. Conclusion

In this study, the performance of BESS in the Korean Peninsula was evaluated with ground based LAI measurement, flux tower measurement and basin-level water balance data and MODIS LAI product was improved. The averages of annual GPP and ET from 2001 to 2011 are 1183 gC m^{-2} $year^{-1}$ and 491 mm $year^{-1}$, respectively. Land cover change is one of main reasons for interannual variation of GPP and ET. Interannual variation of GPP is larger in crop land compared to in forest, while that of ET is smaller in crop land. This seems to be because agricultural activities are mainly controlled by human while forests are not. Biological control such as canopy conductance over ET is dominant in spring and autumn due to spring and autumn drought and summer ET is controlled by available energy and biological factor. ET at high altitude is more sensitive to drought than ET at lowland. The contribution of shaded leaves to GPP is not negligible as shaded leaves contribute to about 51% of summer GPP. .

Reference

Alder, N. N., J. S. Sperry, and W. T. Pockman (1996), Root and stem xylem embolism, stomatal conductance, and leaf turgor in Acer grandidentatum populations along a soil moisture gradient, *Oecologia*, *105*(3), 293-301.

Allen, R. G., M. Tasumi, and R. Trezza (2007), Satellite-based energy balance for mapping evapotranspiration with internalized calibration (METRIC) - Model, *Journal of Irrigation and Drainage Engineering-Asce*, *133*(4), 380-394.

Asner, G. P., J. M. O. Scurlock, and J. A. Hicke (2003), Global synthesis of leaf area index observations: implications for ecological and remote sensing studies, *Global Ecology and Biogeography*, *12*(3), 191-205.

Bae, D. H., I. W. Jung, and H. Chang (2008), Long-term trend of precipitation and runoff in Korean river basins, *Hydrological Processes*, *22*(14), 2644-2656.

Baldocchi, D. (1997), Measuring and modelling carbon dioxide and water vapour exchange over a temperate broad-leaved forest during the 1995 summer drought, *Plant, Cell & Environment*, *20*(9), 1108-1122.

Baldocchi, D., R. Valentini, S. Running, W. Oechel, and R. Dahlman (1996), Strategies for measuring and modelling carbon dioxide and water vapour fluxes over terrestrial ecosystems, *Global Change Biology*, *2*(3), 159-168.

Baldocchi, D., et al. (2001), FLUXNET: A New Tool to Study the Temporal and Spatial Variability of Ecosystem–Scale Carbon Dioxide, Water Vapor, and Energy Flux Densities, *Bulletin of the American Meteorological Society*, *82*(11), 2415-2434.

Brady, N. C., and R. R. Weil (2008), *The Nature and Properties of Soils*, 14 ed., Pearson Prentice Hall, New Jersey.

Bubier, J. L., G. Bhatia, T. R. Moore, N. T. Roulet, and P. M. Lafleur (2003), Spatial and Temporal Variability in Growing-Season Net Ecosystem Carbon Dioxide Exchange at a Large Peatland in Ontario, Canada, *Ecosystems*, *6*(4), 353-367.

Choi, S.-D., K. Lee, and Y.-S. Chang (2002), Large rate of uptake of atmospheric carbon dioxide by planted forest biomass in Korea, *Global Biogeochem. Cycles*,

16(4), 1089.

Cleugh, H. A., R. Leuning, Q. Mu, and S. W. Running (2007), Regional evaporation estimates from flux tower and MODIS satellite data, *Remote Sensing of Environment*, *106*(3), 285-304.

Cramer, W., D. W. Kicklighter, A. Bondeau, B. Moore, G. Churkina, B. Nemry, A. Ruimy, A. L. Schloss, and N. P. P. M. I. Participants Potsdam (1999), Comparing global models of terrestrial net primary productivity (NPP): overview and key results, *Global Change Biology*, *5*, 1-15.

Cramer, W., et al. (2001), Global response of terrestrial ecosystem structure and function to CO2 and climate change: results from six dynamic global vegetation models, *Global Change Biology*, *7*(4), 357-373.

Cressman, G. P. (1959), An operational objective analysis system, *Monthly Weather Review*, *87*(10), 8.

de Pury, D. G. G., and G. D. Farquhar (1997), Simple scaling of photosynthesis from leaves to canopies without the errors of big-leaf models, *de Pury, D. G. G., and G. D. Farquhar*, *Plant, Cell and Environemnt*(20), 21.

Dong, G., J. Guo, J. Chen, G. Sun, S. Gao, L. Hu, and Y. Wang (2011), Effects of spring drought on carbon sequestration, evapotranspiration and water use efficiency in the songnen meadow steppe in northeast China, *Ecohydrology*, *4*(2), 211-224.

Fang, H., S. Liang, J. Townshend, and R. Dickinson (2008), Spatially and temporally continuous LAI data sets based on an integrated filtering method: Examples from North America, *Remote Sensing of Environment*, *112*(1), 75-93.

Fang, H., S. Liang, H.-Y. Kim, J. R. Townshend, C. L. Schaaf, A. H. Strahler, and R. E. Dickinson (2007), Developing a spatially continuous 1 km surface albedo data set over North America from Terra MODIS products, *Journal of Geophysical Research*, *112*(D20).

Farquhar, G. D., S. v. Caemmerer, and J. A. Berry (1980), A biochemical model of photosynthetic CO2 assimilation in leaves of C3 species, *Planta*, *149*, 13.

Friedl, M. (n.d.), Land Cover Type Yearly L3 Global 500 m SIN Grida, edited, U.S. Geological Survey, .

Friedl, M. A., D. Sulla-Menashe, B. Tan, A. Schneider, N. Ramankutty, A. Sibley, and X. Huang (2010), MODIS Collection 5 global land cover: Algorithm refinements and characterization of new datasets, *Remote Sensing of Environment*, *114*(1), 168-182.

Heinsch, F. A., et al. (2006), Evaluation of remote sensing based terrestrial productivity from MODIS using regional tower eddy flux network observations, *Ieee Transactions on Geoscience and Remote Sensing*, *44*(7), 1908-1925.

Hong, J., and J. Kim (2011), Impact of the Asian monsoon climate on ecosystem carbon and water exchanges: a wavelet analysis and its ecosystem modeling implications, *Global Change Biology*, *17*(5), 1900-1916.

Hong, J., J. Kim, D. Lee, and J.-H. Lim (2008), Estimation of the storage and advection effects on H2O and CO2 exchanges in a hilly KoFlux forest catchment, *Water Resour. Res.*, *44*(1), W01426.

Hoover, C. M. (2008), Field Measurements for Forest Carbon Monitoring, edited, p. 240, Springer, New York, USA.

Hwang, T., S. Kang, J. Kim, Y. Kim, D. Lee, and L. Band (2008), Evaluating drought effect on MODIS Gross Primary Production (GPP) with an eco-hydrological model in the mountainous forest, East Asia, *Global Change Biology*, *14*(5), 1037-1056.

Iwabuchi, H. (2006), Efficient Monte Carlo Methods for Radiative Transfer Modeling, *Journal of the Atmospheric Sciences*, *63*(9), 2324-2339.

Jönsson, P., and L. Eklundh (2004), TIMESAT—a program for analyzing time-series of satellite sensor data, *Computers & Geosciences*, *30*(8), 833-845.

Jung, M., et al. (2010), Recent decline in the global land evapotranspiration trend due to limited moisture supply, *Nature*, *467*(7318), 951-954.

Kang, M., H. Kwon, J. H. Cheon, and J. Kim (2012), On Estimating Wet Canopy Evaporation from Deciduous and Coniferous Forests in the Asian Monsoon

Climate, *Journal of Hydrometeorology*, *13*(3), 950-965.

Khatun, R., et al. (2011), Spatial variations in evapotranspiration over East Asian forest sites. II. Surface conductance and aerodynamic conductance, *Hydrological Research Letters*, *5*, 88-92.

Kim, Y., S. Kang, J.-H. Lim, D. Lee, and J. Kim (2010), Inter-annual and inter-plot variations of wood biomass production as related to biotic and abiotic characteristics at a deciduous forest in complex terrain, Korea, *Ecological Research*, *25*(4), 757-769.

Kobayashi, H., and D. G. Dye (2005), Atmospheric conditions for monitoring the long-term vegetation dynamics in the Amazon using normalized difference vegetation index, *Remote Sensing of Environment*, *97*(4), 519-525.

Kobayashi, H., and H. Iwabuchi (2008), A coupled 1-D atmosphere and 3-D canopy radiative transfer model for canopy reflectance, light environment, and photosynthesis simulation in a heterogeneous landscape, *Remote Sensing of Environment*, *112*(1), 173-185.

Kottek, M., J. Grieser, C. Beck, B. Rudolf, and F. Rubel (2006), World Map of the Köppen-Geiger climate classification updated, *Meteorologische Zeitschrift*, *15*(3), 259-263.

Kwon, H., J. Kim, J. Hong, and J. H. Lim (2010), Influence of the Asian monsoon on net ecosystem carbon exchange in two major ecosystems in Korea, *Biogeosciences*, *7*(5), 1493-1504.

Kwon, H., T.-Y. Park, J. Hong, J.-H. Lim, and J. Kim (2009), Seasonality of Net Ecosystem Carbon Exchang in Two Major Plant Functional Types in Korea, *Asia-Pacific Journal of Atmospheric Sciences*, *45*(2), 149-163.

Lee, D., J. Kim, K. S. Lee, and S. Kim (2010), Partitioning of catchment water budget and its implications for ecosystem carbon exchange, *Biogeosciences*, *7*(6), 1903-1914.

Leuning, R., F. M. Kelliher, D. G. G. De Pury, and E. D. Schulze (1995), Leaf nitrogen, photosynthesis, conductance and transpiration: scaling from leaves to

canopies, *Plant, Cell & Environment*, *18*(10), 1183-1200.

Mu, Q., F. A. Heinsch, M. Zhao, and S. W. Running (2007), Development of a global evapotranspiration algorithm based on MODIS and global meteorology data, *Remote Sensing of Environment*, *111*(4), 519-536.

Myneni, R. B., et al. (2002), Global products of vegetation leaf area and fraction absorbed PAR from year one of MODIS data, *Remote Sensing of Environment*, *83*(1-2), 214-231.

Norman, J. M., W. P. Kustas, and K. S. Humes (1995), Source approach for estimating soil and vegetation energy fluxes in observations of directional radiometric surface temperature, *Agricultural and Forest Meteorology*, *77*(3–4), 263-293.

Qiu, Y., B. Fu, J. Wang, and L. Chen (2001), Spatial variability of soil moisture content and its relation to environmental indices in a semi-arid gully catchment of the Loess Plateau, China, *Journal of Arid Environments*, *49*(4), 723-750.

Ranga Myneni, R. (n.d.), Leaf Area Index - Fraction of Photosynthetically Active Radiation 8-Day L4 Global 1km, edited, U.S. Geological Survey, .

Rodell, M., J. S. Famiglietti, J. Chen, S. I. Seneviratne, P. Viterbo, S. Holl, and C. R. Wilson (2004), Basin scale estimates of evapotranspiration using GRACE and other observations, *Geophysical Research Letters*, *31*(20).

Running, S. W., D. D. Baldocchi, D. P. Turner, S. T. Gower, P. S. Bakwin, and K. A. Hibbard (1999), A Global Terrestrial Monitoring Network Integrating Tower Fluxes, Flask Sampling, Ecosystem Modeling and EOS Satellite Data, *Remote Sensing of Environment*, *70*(1), 108-127.

Ryu, Y., et al. (2011), Integration of MODIS land and atmosphere products with a coupled-process model to estimate gross primary productivity and evapotranspiration from 1 km to global scales, *Global Biogeochemical Cycles*, *25*(4).

Schmid, H. P. (1994), SOURCE AREAS FOR SCALARS AND SCALAR FLUXES, *Boundary-Layer Meteorology*, *67*(3), 293-318.

Schwarz, M., and N. E. Zimmermann (2005), A new GLM-based method for mapping tree cover continuous fields using regional MODIS reflectance data, *Remote Sensing of Environment*, *95*(4), 428-443.

Sims, D., A. Rahman, V. Cordova, B. Elmasri, D. Baldocchi, P. Bolstad, L. Flanagan, A. Goldstein, D. Hollinger, and L. Misson (2008), A new model of gross primary productivity for North American ecosystems based solely on the enhanced vegetation index and land surface temperature from MODIS, *Remote Sensing of Environment*, *112*(4), 1633-1646.

Sitch, S., et al. (2008), Evaluation of the terrestrial carbon cycle, future plant geography and climate-carbon cycle feedbacks using five Dynamic Global Vegetation Models (DGVMs), *Global Change Biology*, *14*(9), 2015-2039.

Sprintsin, M., J. M. Chen, A. Desai, and C. M. Gough (2012), Evaluation of leaf-to-canopy upscaling methodologies against carbon flux data in North America, *J. Geophys. Res.*, *117*(G1), G01023.

Su, Z. (1999), The Surface Energy Balance System (SEBS) for estimation of turbulent heat fluxes, *Hydrol. Earth Syst. Sci.*, *6*(1), 16.

Tan, B., C. E. Woodcock, J. Hu, P. Zhang, M. Ozdogan, D. Huang, W. Yang, Y. Knyazikhin, and R. B. Myneni (2006), The impact of gridding artifacts on the local spatial properties of MODIS data: Implications for validation, compositing, and band-to-band registration across resolutions, *Remote Sensing of Environment*, *105*(2), 98-114.

Turner, D. P., S. V. Ollinger, and J. S. Kimball (2004), Integrating Remote Sensing and Ecosystem Process Models for Landscape- to Regional-Scale Analysis of the Carbon Cycle, *BioScience*, *54*(6), 573-584.

Turner, D. P., S. Urbanski, D. Bremer, S. C. Wofsy, T. Meyers, S. T. Gower, and M. Gregory (2003), A cross-biome comparison of daily light use efficiency for gross primary production, *Global Change Biology*, *9*(3), 383-395.

Verger, A., F. Baret, and M. Weiss (2011), A multisensor fusion approach to improve LAI time series, *Remote Sensing of Environment*, *115*(10), 2460-2470.

Willmott, C. J. (1982), Some Comments on the Evaluation of Model Performance, *Bulletin of the American Meteorological Society*, *63*(11), 1309-1313.

Wittig, V. E., C. J. Bernacchi, X.-G. Zhu, C. Calfapietra, R. Ceulemans, P. Deangelis, B. Gielen, F. Miglietta, P. B. Morgan, and S. P. Long (2005), Gross primary production is stimulated for three Populus species grown under free-air CO2 enrichment from planting through canopy closure, *Global Change Biology*, *11*(4), 644-656.

Wu, C., J. W. Munger, Z. Niu, and D. Kuang (2010), Comparison of multiple models for estimating gross primary production using MODIS and eddy covariance data in Harvard Forest, *Remote Sensing of Environment*, *114*(12), 2925-2939.

Yeh, P. J.-F., M. Irizarry, and E. A. B. Eltahir (1998), Hydroclimatology of Illinois: A comparison of monthly evaporation estimates based on atmospheric water balance and soil water balance, *J. Geophys. Res.*, *103*(D16), 19823-19837.

Yuan, H., Y. Dai, Z. Xiao, D. Ji, and W. Shangguan (2011), Reprocessing the MODIS Leaf Area Index products for land surface and climate modelling, *Remote Sensing of Environment*, *115*(5), 1171-1187.

Yuan, W., et al. (2010), Global estimates of evapotranspiration and gross primary production based on MODIS and global meteorology data, *Remote Sensing of Environment*, *114*(7), 1416-1431.

Zhang, F., J. M. Chen, J. Chen, C. M. Gough, T. A. Martin, and D. Dragoni (2012), Evaluating spatial and temporal patterns of MODIS GPP over the conterminous U.S. against flux measurements and a process model, *Remote Sensing of Environment*, *124*, 717-729.

Zhang, J.-H., S.-J. Han, and G.-R. Yu (2006a), Seasonal variation in carbon dioxide exchange over a 200-year-old Chinese broad-leaved Korean pine mixed forest, *Agricultural and Forest Meteorology*, *137*(3–4), 150-165.

Zhang, J., G. Yu, S. Han, D. Guan, and X. Sun (2006b), Seasonal and annual variation of CO2 flux above a broad-leaved Korean pine mixed forest, *SCI CHINA SER D*, *49*(2), 63-73.

Zhao, M. S., F. A. Heinsch, R. R. Nemani, and S. W. Running (2005), Improvements of the MODIS terrestrial gross and net primary production global data set, *Remote Sensing of Environment*, *95*(2), 164-176.

초록

BESS 를 이용한 한반도의 광합성과 증발산의 시공간 패턴 분석

전 수 현

환경계획학과

서울대학교 환경대학원

육상생태계에서의 탄소와 물 순환을 이해하고, 탄소와 물 순환의 변화를 예측하기위해서는 광합성과 증발산의 시공간적인 패턴을 분석하는 것이 중요하다. 하지만 시공간적으로 연속된 광합성량과 증발산량을 한반도내에서 추정한 연구는 거의 없었다. 이 연구에서는 생물리모형인 Breathing Earth System Simulator (BESS)를 이용해 한반도 내의 광합성과 증발산의 시공간적인 패턴을 분석하였다.

엽면적지수(Leaf Area Index, LAI)는 BESS 모형의 가장 중요한 입력변수 중 하나로, BESS 모형에서 광합성과 증발산은 엽면적지수에 가장

민감도가 높다. 엽면적지수 보정은 re-modified temporal and spatial filter (rTSF) 방법을 통해 이루어졌다. 엽면적지수 보정결과 BESS의 것과 raw MODIS의 것보다 정확도가 향상되었다. 2001부터 2011년까지 한반도의 광합성과 증발산 추정은 보정된 엽면적지수를 이용하였다. BESS를 통해 얻어진 광합성과 증발산은 각각 4군데와 5군데 사이트에서 에디공분산을 통해 관측된 측정값을 통해 평가되었다. 또한, 물수지방법을 이용한 유역규모의 증발산량을 추정하여, BESS의 결과값을 평가하였다. GDK와 GCK사이트에서는 현장관측값에 비해 BESS의 광합성과 증발산이 모두 양으로 편중되어 있었으나, 다른 사이트에서는 현장관측결과와 BESS의 결과들이 비슷한 값을 보였다.

2001년부터 2011년까지 평균 연 광합성과 증발산량은 각각 1,183 gC m^{-2} $year^{-1}$과 491 mm $year^{-1}$이었다. 광합성과 증발산의 연간변화의 주된 원인중 하나는 토지피복변화였다. 고지대에서의 증발산은 평년에 비해 건조한 해에 canopy conductance에 더 민감하게 반응하였다. 봄 가뭄과 가을 가뭄은 봄과 가을 증발산이 canopy conductance에 더 민감하게 반응하는 원인이었다. 여름철 가뭄으로 인한 구름양 증가로 인해, 여름에는 가용한 에너지가 증발산을 좌우하는 주요 요소로 작용하였다.

주요어: 광합성, 증발산, Breathing Earth System Simulator (BESS), Flux tower

Acknowledgements

This study was supported by Korea-Americas Cooperation Program through the National Research Foundation of Korea (NRF) funded by the Korean Ministry of Education, Science and Technology (2011–0030485). The flux tower data of GDK and GCK from 2005 to 2007 were provided by KoFlux from the projects funded by Ministry of Land, Transport and Maritime Affairs, Ministry of Environment, and Korea Science and Engineering Foundation. The flux tower data of GDK and GCK in 2008 were provided by KoFlux from the projects funded by Ministry of Land, Transport and Maritime Affairs and Korea Science and Engineering Foundation. The flux tower data of GDK and GCK from 2009 to 2011 were provided by KoFlux from the projects funded by Korea Forest Research Institute and the A3 program of National Research Foundation of Korea. The flux tower data of HFK from 2004 to 2007 were provided by KoFlux from the projects funded by Ministry of Land, Transport and Maritime Affairs, Ministry of Environment, and Korea Meteorological Administration. The flux tower data of HFK from 2008 to 2011 were provided by KoFlux from the projects funded by Korea Meteorological Administration and the A3 program of National Research Foundation of Korea. The flux tower data of SMK and CRK from 2007 to 2011 were provided by KoFlux from the project funded by Hydrological Survey Center.